Biogeosciences Open Access
Discussions
EGU

The recent state and variability of the carbonate system of the Canadian Arctic in the context of ocean acidification

Alexis Beaupré-Laperrière[1], Alfonso Mucci[1] and Helmuth Thomas[2]

[1]GEOTOP and Department of Earth and Planetary Sciences, McGill University, 3450 University
5 Street, Montreal, Quebec, H3A 0E8, Canada

[2]Dalhousie University, Department of Oceanography, Halifax, NS, Canada (now at Center for Materials and Coastal Research, Helmholtz-Zentrum Geesthacht, Germany)

Correspondence to: Alexis Beaupré-Laperrière (alexis.beauprelaperriere@mail.mcgill.ca)

10

Abstract

Ocean acidification driven by the uptake of anthropogenic CO_2 by the surface oceans constitutes a potential threat to the health of marine ecosystems around the globe. The Arctic Ocean is particularly vulnerable to acidification due to its relatively low buffering capacity and, thus, is
15 an ideal region to study the progression and effects of acidification before they become globally widespread. The appearance of undersaturated surface waters with respect to the carbonate mineral aragonite ($\Omega_A < 1$), an important threshold beyond which the calcification and growth of some marine organisms might be hindered, has recently been documented in the Canada Basin and adjacent Canadian Arctic Archipelago. Nonetheless, few of these observations were made in the
20 last five years and the spatial coverage in the latter region is poor. Additionally, the strong variability inherent to this dynamic shelf environment renders the temporal imprint of ocean acidification on carbonate system parameters (pH, pCO_2, DIC, Ω) virtually indistinguishable on decadal timescales. We use a dataset of carbonate system parameters measured in Canadian Arctic Archipelago (CAA) and its adjacent basins to describe the recent state of these parameters across
25 the Canadian Arctic and investigate the amplitude and sources of the system's variability. Our findings reveal that, in addition to the surface of the Canada Basin, the entire water column of the Queen Maud Gulf was undersaturated with respect to aragonite in 2015 and 2016. We also estimate that approximately a third of the interannual variability in surface DIC in the CAA results from fluctuations in biological activity.

30

Biogeosciences

Discussions

Open Access

EGU

1 Introduction

Ocean acidification and its repercussions on marine ecosystems constitute an important consequence of the ongoing rise in atmospheric carbon dioxide (CO_2) concentrations. The world's oceans absorbed approximately a third of the anthropogenic CO_2 released to the atmosphere over

35   the last two centuries of industrial activity (Sabine et al., 2004) and are currently a sink for ~24% of global annual anthropogenic carbon emissions (Le Quéré et al., 2018). Atmospheric carbon dioxide uptake by the surface oceans has well defined impacts on seawater chemistry, including a decrease of pH resulting from the dissociation of carbonic acid (H_2CO_3), the product of the reaction between water and dissolved CO_2. A large fraction of the hydrogen ions released by this reaction

40   is neutralized by carbonate ions (CO_3^{2-}), leading to a decrease of their concentration and, concomitantly, the saturation state of seawater with respect to the carbonate minerals calcite and aragonite. The saturation state is defined by:

(1) $\Omega_{C,A} = [Ca^{2+}][CO_3^{2-}] / K^*_{SP}$

where square brackets denote concentrations and K^*_{SP} is the stoichiometric solubility product of

45   calcite or aragonite, the two most common marine $CaCO_3$ polymorphs, at a given temperature, pressure and salinity.

The combination of these phenomena is most often referred to as ocean acidification (OA). As it proceeds, the dissolved inorganic carbon concentration (DIC; the sum of $[H_2CO_3^*]$, $[HCO_3^-]$

50   ] and $[CO_3^{2-}]$) in the surface ocean is expected to increase relative to the total alkalinity (TA; the capacity of a solution to neutralize protons), as the latter is nearly conservative in the surface ocean (Wolf-Gladrow et al., 2007). The global mean surface ocean pH currently sits ~0.1 units below its preindustrial value (Orr et al., 2005) and, according to Earth System models, under the IPCC's "business as usual" RCP8.5 emission scenario, is predicted to decrease by an additional 0.3 units

55   by the end of this century (Bopp et al., 2013).

Marine calcifying organisms, many of which are important primary producers (e.g., coccolithophores), extract the constituents of their calcitic or aragonitic tests (shells) from seawater. In most cases, their ability to do so is directly dependent on the saturation state of the

60   surrounding water. Supersaturated seawater ($\Omega > 1$) will favor carbonate precipitation whereas undersaturated seawater ($\Omega < 1$) favors carbonate dissolution. The majority of calcifying organisms, such as planktonic foraminifera and coccolithophores, undergo dissolution or exhibit substantially hindered growth when exposed to undersaturated seawater (e.g., Mostofa et al., 2016). Calcifying organisms found in the Arctic Ocean are subject to rapid environmental changes,

65   as this polar ocean is warming more rapidly than others (Serreze et al., 2011) and is particularly vulnerable to acidification due to the low alkalinity and correspondingly weak buffer capacity of its cold waters (Shadwick et al., 2013). Atmospheric CO_2 uptake by Arctic surface waters is further promoted by the rapidly melting seasonal ice cover (e.g., Stroeve et al., 2012), which exposes a gradually larger area of the ocean to gas exchange with the atmosphere and whose melt-water

70   dilutes calcium concentrations, alkalinity and carbonate ion concentrations, further decreasing Ω.

        The Canadian Arctic Archipelago (CAA) and its adjacent deep basins, the Canada Basin (CB) and Baffin Bay (BB, Fig. 1), are part of the region projected to undergo the largest reduction in ice cover and, consequently, the largest decrease in surface pH (~0.6) and Ω (1 and 0.7 for Ω_C

75   and Ω_A, respectively) over the 21st century (Popova et al., 2014). Recent observations (e.g. Yamamoto-Kawai et al., 2009b; Robbins et al., 2013; Qi et al., 2017) hint at a significant decrease of the aragonite saturation state of surface waters as well as a rapid expansion of the undersaturated area in the Canada Basin, but most of these time series predate 2010 and do not extend geographically to the CAA and Baffin Bay.

80

        In this study, we use a large observational dataset for this part of the Arctic to 1) describe the recent state of the carbonate chemistry and its spatial variability in the Canadian Arctic Archipelago and the adjacent basins, 2) investigate the interannual variability in carbonate system parameters and identify detectable temporal trends using time series spanning from 2003 to 2016

85   and 3) estimate the contribution of the temporal change in biological activity to the observed variability of surface DIC.

2 Study area

2.1 Canada Basin

The Canada Basin (CB), Canadian Arctic Archipelago and Baffin Bay accommodate the flow of surface waters from the North Pacific to the North Atlantic (Stigebrandt, 1984), as well as circulation of Atlantic waters at greater depths. The water mass structure of the southern Canada Basin is representative of these broad circulation patterns and can be summarized as follows (Carmack et al., 1989; MacDonald et al., 1989; Lansard et al., 2012): a relatively cold and fresh surface layer that contains significant fractions of meteoric water (river discharge and precipitation) and sea-ice melt in the summer and becomes homogeneous in winter; an intermediate layer (~50-200m) of advected Pacific waters, often divided into summer and winter varieties, the latter being distinctively rich in nutrients and metabolic CO_2 and recognizable by a temperature minimum in the upper halocline; a layer of warm (~0.5°C) and saline ($S_P>34$) Atlantic water; a cold bottom layer with practical salinities (S_P) reaching 34.85. The main surface circulation feature in this area, the clockwise Beaufort Gyre, is the largest freshwater reservoir in the northern oceans, formed through Ekman pumping (Proshutinsky et al., 2009). This feature is reversed at depth. The main source of freshwater to the Beaufort Sea (the southwest portion of the Canada Basin) is the Mackenzie River (Carmack and MacDonald, 2002), although the contribution of sea-ice melt is significantly increasing along with the accelerating reduction in ice cover (Yamamoto-Kawai et al., 2009a). The supply of freshwater at the surface, combined with the advection of pre-acidified waters from the Pacific (100-200 m) and the Atlantic (below 400 m; Luo et al., 2016) Oceans result in the presence of three distinct and expanding undersaturation horizons in the Canada Basin (Wynn et al., 2016).

2.2 Canadian Arctic Archipelago

The CAA is a series of islands on the Canadian continental shelf, through which complex circulation patterns unfold in narrow and relatively shallow channels (<500 m). See McLaughlin et al. (2004) for a detailed description of the circulation and water mass processes in this area. The prominent pathway for the eastward flow of Canada Basin water masses into Baffin Bay extends along the 74th parallel from M'Clure Strait to Lancaster Sound. A shallow 125-m sill at Barrow

Strait, located centrally in the archipelago, inhibits the eastward flow of Atlantic waters, so that only surface and Pacific-origin waters reach Baffin Bay (Bidleman et al., 2007). The properties of

120   these water masses are substantially modified during this transit (McLaughlin et al., 2004). East of Barrow Strait, Atlantic waters originating from the Labrador Sea penetrate the archipelago through Baffin Bay. Smaller inflows of water from the deep Arctic Ocean into the archipelago occur through the Queen Elizabeth Islands (North-East) and Nares Strait; minor outflows occur through Jones Sound and into Hudson Bay via Foxe Basin. Notwithstanding the Mackenzie River,

125   whose discharge is limited to the Beaufort Sea and Amundsen Gulf, the southern portion of the CAA receives a considerable amount of freshwater from other large North American rivers (e.g., Coppermine, Burnside, Black).

2.3 Baffin Bay

130   The oceanographic regime of Baffin Bay is distinct from that of the CAA and CB, as it receives multiple inputs from both the Arctic and Atlantic Oceans. Cold and relatively fresh Arctic and Pacific-derived waters enter this 2300-m deep semi-enclosed basin through the Nares Strait as well as Jones and Lancaster Sounds (Muench, 1971; Jones et al., 1998, 2003). Warmer and more saline Atlantic Ocean waters are transported from the Labrador Sea by the West Greenland Current (WGC) into Baffin Bay through the eastern side of Davis Strait, circulate cyclonically, i.e., in an

135   anti-clockwise direction, before joining the southward Baffin Island Current (BIC) which exits Baffin Bay through the western Davis Strait (Bourke et al., 1989, Munchow et al., 2015). Atlantic Ocean waters are modified as they mix with Arctic inflows in Northern Baffin Bay, near the North Water Polynya (Melling et al., 2001). The resulting water mass structure is described by Tang et

140   al. (2004) as: 1) a cold (T<0°C) and relatively fresh (S_P<33.7) surface layer, representing the mixed Arctic inputs, 2) a warm (T>0°C) and saline (S_P>34) Atlantic Ocean water layer found at depths of ~300 to 800 m, and 3) a deeper layer of nearly constant salinity (S_P = 34.5).

145

3 Methods

The dataset used in this study comprises data from 420 stations visited during various research cruises carried out aboard the CCGS Amundsen between 2003 and 2016. Table 1 summarizes the timeframe and relevant data acquired during each cruise; figure 2 shows the position of each sampling station. Although ice conditions restricted most observations to the summer months, two winter time-series, acquired in 2003-2004 (CASES, Miller et al., 2011) and 2007-2008 (CFL, Shadwick et al., 2011) are included in the dataset.

3.1 Sampling and measurements

Seawater was sampled separately for each measured parameter from Niskin bottles mounted on a Rosette system equipped with a Seabird SBE 911plus Conductivity-Temperature-Depth (CTD) sensor, which collected *in-situ* practical salinity (S_P) and temperature data throughout the water column. The conductivity/salinity probe was calibrated post-cruise against measurements carried out on discrete seawater samples using a Guildline Autosal 8400 salinometer (accuracy of ± 0.002 or less), itself calibrated with IAPSO standard seawater. Samples used for pH determination were drawn directly from the Niskin bottles into 125 mL low density polyethylene (LDPE) bottles with no headspace to avoid gas exchange with surrounding air and left to thermally equilibrate in a temperature bath set at 25.0 (±0.1) °C. pH, on the total proton scale (pH_T), was then measured spectrophometrically on a Hewlett-Packard 8453 UV-visible diode array spectrophotometer using m-Cresol purple (Clayton and Byrne, 1993) and Phenol red (Robert-Baldo et al., 1985) indicators at 434 and 578 nm or 433 and 558 nm, respectively, in a 5-cm quartz cell. Daily calibrations were performed with TRIS buffer solutions at practical salinities of 25 and/or 35, depending on the salinity range of the samples. The reproducibility was found to be ±0.005 pH units or better, based on duplicate measurements of the same samples with the same or both indicators. Samples destined for total alkalinity (TA) and dissolved inorganic carbon (DIC) analyses were drawn directly from the Niskin bottles into 250 or 500 mL glass bottles with ground-glass stoppers, poisoned with solid mercuric chloride ($HgCl_2$) to halt biological activity, and sealed with Apiezon M grease.

175   TA and DIC from the GEOTRACES 2009 and all post-2010 cruises were measured onboard or at Dalhousie University on a Marianda VINDTA 3C instrument, following the protocol described by Dickson et al. (2007) and calibrated with Certified Reference Materials (CRM) provided by A.G. Dickson (Scripps Institute of Oceanography). The precision of the instrument was found to be $\pm$ 2-3 µmol kg^{-1} based on repeated CRM analyses. The remaining DIC and TA

180   analyses were performed respectively on a SOMMA instrument (Johnson et al., 1993) fitted to a UIC 5011 coulometer and by potentiometric titration using a Radiometer Titrilab 865 (see Mucci et al., 2010 for details), calibrated against the same CRMs used with the VINDTA.

In-situ pH_T, DIC (ArcticNet 2009 only), pCO_2, Ω_C and Ω_A, were calculated from TA and

185    $pH_T(25°C)$ or TA and DIC (for 548 out of 4730 data points) with the Excel - 2.1 version of the CO2SYS algorithm (Lewis and Wallace, 1998), using the carbonic acid dissociation constants determined by Mehrbach et al. (1973), refit by Dickson and Millero, (1987), the HSO_4^- dissociation constants of Dickson (1990) and the total boron concentration (B_T) from Uppström (1974). pCO_2 was normalized, using CO2SYS, to the mean temperature of the top 100 meters of the water

190   column (-0.4 °C). The resulting $\partial pCO_2 /\partial T/pCO_2$ values range between 0.033 and 0.051 °C^{-1}, with a mean of 0.046 °C^{-1}, in good agreement with values obtained by Jiang et al. (2008; 0.027-0.042°C^{-1}) and Takahashi et al. (1993; 0.0423 °C^{-1}).

3.2 Quality control

195   In order to assess the robustness of the computed DIC values, we calculated DIC from TA and $pH_T(25°C)$ and compared the results with the measured DIC values. The resulting coefficient of determination of the linear fit to the measured and calculated DIC values, R^2, is 0.989, while the mean difference between calculated and measured DIC values is ~2 µmol kg^{-1}. We excluded 30 measurements that differed from the calculated values by more than 50 µmol kg^{-1} (2.5% of the

200   mean DIC).

Questionable TA measurements, excluded from the dataset, were identified as those outside a range of 3 standard deviations from the mean salinity-normalized TA for individual regions (CB, CAA, BB) characterized by internally consistent water mass assemblages. TA measurements obtained from the two instrumental methods (VINDTA and Radiometer Titrilab 865) used in 2015 and 2016 were also compared to ensure that data originating from both methods could be used interchangeably in the calculation of additional parameters and conjointly in time series. The resulting coefficient of determination between both datasets (R^2) is 0.988, the mean of the non-systematic discrepancy between values is 6 µmol kg^{-1} and its maximum is 36 µmol kg^{-1}, respectively corresponding to 0.3% and 1.7% of the mean TA. The degree to which the results of this test are representative of the entire dataset is uncertain, but they constitute the best possible estimate of the uncertainty associated with the use of the two analytical methods used to measure TA. When TA measurements obtained from both methods deviated significantly (>10 µmol kg^{-1}), specific alkalinity (TA/S_P), which should remain relatively constant in a given water mass of uniform salinity (Millero, 2005; p.268), was used to determine which data to discard. The deviation from TA values calculated from DIC and $pH_T(25°C)$ was used to complement the first method, especially at the surface, although the validity of DIC measurements was previously assessed using TA.

3.3 Error estimation

In order to quantify the error associated with the calculated carbonate system parameters reported in this study, we used the CO2SYS program modified by Orr et al. (2018), which applies error propagation to instrumental and constant-related uncertainties. For simplicity, we report the mean uncertainty for each parameter (see Table 2), as the variance is minimal within our dataset. We found the additional uncertainty associated with the unavailability of nutrient concentrations (P and Si) as input parameters in CO2SYS to be negligible (up to 0.0006 pH units, 1.5 µatm pCO_2 and 0.006 Ω units, as determined using nutrient data where available). The uncertainty on Δ DIC_{Bio}, the biological contribution to temporal variations of the surface DIC pool, was calculated by applying standard error propagation to the procedure described in Sect. 4.3.

Biogeosciences
Discussions

4 Results and discussion

4.1 Recent observations (2014-2016)

4.1.1 Surface observations

To characterize the recent state of seawater carbonate chemistry in the study area, we use data

235   obtained in the late summers (August - September) of 2014, 2015 and 2016. Uncertainties for each

parameter can be found in the Methods (Sect. 3.3). The mean 2014-2016 surface (< 10 m) practical

salinity (S_P), TA and DIC values in the Canada Basin (CB), Canadian Arctic Archipelago (CAA)

and Baffin Bay (BB) are presented in Table 3. It is important to note that the mean regional values

we report for the Canada Basin may be skewed by the higher density of stations located along the

240   Mackenzie Shelf, and that our sample size for Baffin Bay consists of only 6 stations. Practical

salinities considerably below 25 were mostly observed near the mouth of the Mackenzie River,

with some in the Queen Maud Gulf (QMG). The discrepancy between S_P and TA values observed

in the CB/CAA and Baffin Bay clearly illustrates the change in water mass regime west of

Lancaster Sound (see Sect. 2), while DIC, which is strongly affected by biological activity, shows

245   a less prominent spatial pattern. In all regions, surface-water pCO_2, of which we only consider

data acquired over the top 5 meters of the water column in order to render it more indicative of gas

exchange potential, was largely undersaturated with respect to the atmosphere, by as much as 150

μatm (Fig. 3). This suggests that the region as a whole acts as a net CO_2 sink during the summer,

as Geilfus et al. (2018) observed in 2011. Ahmed et al. (2019) came to a similar conclusion based

250   on underway pCO_2 measurements carried out in the CAA between 2010 and 2016, but reported

consistent temporal fluctuations of summer sea-surface pCO_2 and ΔpCO_2 driven by sea-ice

processes. The handful of locations exhibiting a positive ΔpCO_2 ($pCO_{2SW} - pCO_{2air}$; outgassing to

the atmosphere) are located in the QMG and the transect between Banks Island and Cape Bathurst

(Fig. 4), where the episodic upwelling of upper halocline water is well documented (Mucci et al.,

255   2010; Tremblay et al., 2011).

The saturation state of surface waters (<10m) with respect to aragonite (Ω_A, Fig. 5) ranges

from 0.82 to 2.03 (mean 1.26), 0.73 to 2.01 (mean 1.22) and 1.47 to 1.69 (mean 1.57) respectively

in the CB, CAA and BB. Ω_A correlates well with S_P (r=0.79; Fig. 6), although the surface samples

260   with the highest salinities (S_P ~32), collected in Baffin Bay, were not the most supersaturated.

Recurrent undersaturated conditions ($\Omega_A < 1$), potentially deleterious to calcifying organisms, are found at the surface in two areas: the central Canada Basin and the Queen Maud Gulf. Such conditions have been well documented in the former (e.g., Robbins et al., 2013), and attributed mostly to the input of sea-ice melt, which lowers Ω_A by diluting surface waters and promotes CO_2

265   uptake (Yamamoto-Kawai et al., 2011). As of 2016, surface undersaturation with respect to aragonite was limited to the central Canada Basin and did not extend to its bordering continental shelf, where Ω_A remains near saturation (1-1.25).

In the Queen Maud Gulf, surface Ω_A values as low as 0.84 and 0.73 (±0.16) were observed in

270   2015 and 2016, respectively (most visible as the two minima in Fig. 6). Most of the surrounding samples were slightly undersaturated ($\Omega_A \sim 0.90$ -1.05). Both minima were associated with locally higher pCO_2 values (~429 and 438 ± 6 µatm) and practical salinities of 26.54 and 22.17. Two mechanisms, namely the decrease in the calcium (Ca^{2+}) ion concentration and alkalinity via dilution by freshwater and the decrease of the CO_3^{2-} concentration concomitant with a decrease in

275   pH, explain these saturation minima. The former process is self-explanatory and results from the documented increase in freshwater inputs by melting of sea-ice (Yamamoto-Kawai et al., 2009b) and increased river discharge (Déry et al., 2016). We estimate, based on a linear regression of surface $\delta^{18}O$ data against S_P, that upwards of 95% of the freshwater at the surface of the QMG in 2015 was of riverine origin (Appendix B). Our dataset does not allow us to directly differentiate

280   the contributions of air-sea gas exchange and biological activity (respiration) to the high pCO_2 observed at these locations. Nonetheless, the depth of these samples (<5 m) implies some degree of equilibration with the atmosphere. Although the diurnal cycle of biological activity may play a role in the development of peaks in Ω, we rule out this mechanism for the case discussed above, as the 0.73 minimum of 2016 was observed in the early afternoon. Although the Ω_A minima

285   represent significant undersaturation, the uncertainty on Ω_A computations (0.08 or 0.16 depending on the parameters used in the calculation; see Methods) blurs the saturation threshold in such a way that Ω_A values marginally below 1 might in reality represent supersaturated conditions, and vice-versa. It is important to note that, even without the influence of climate change, areas of high riverine discharge naturally harbor lower carbonate mineral saturation states. Thus, undersaturated

290   conditions in the QMG and elsewhere do not solely result from the documented increase of

freshwater inputs described above. Nonetheless dilution by freshwater affects the degree of this undersaturation as well as its spatial and temporal extent.

295   Surface waters throughout the study area are supersaturated with respect to calcite, with Ω_C ranges (mean) of 1.34 to 3.25 (2.04), 1.21 to 3.29 (1.97) and 2.38 to 2.70 (2.52) in the CB, CAA and BB, respectively. Uncertainties on Ω_C values are on the order of 0.25-0.30, almost twice as large as those of Ω_A, due to the larger uncertainty of the calcite stoichiometric solubility product at 25 °C and $S_P = 35$ (Mucci, 1983).

300   **4.1.2 Water column observations**

Depth profiles of pH_T, pCO_2 and Ω_A grouped by region (equivalent to water-mass regime) are presented in Fig. 7. We divided the broad Canadian Arctic Archipelago region into four sub-regions (see Fig. 2): The Parry Channel, the east-west channel extending from M'Clure Strait to Lancaster Sound, the Amundsen Gulf, the Queen Maud Gulf and the central CAA, which connects
305   the QMG to the Parry Channel. The water mass structures are essentially the same as those described in Sect. 2.

The most prominent feature in profiles of carbonate system parameters in the Canada Basin is the Upper Halocline Layer (UHL), a layer of water originating from the Pacific Ocean with a
310   relatively lower pH due to its high metabolic CO_2 content (Shadwick et al., 2011). In 2014-2016, the UHL was characterized by a pH_T minimum of 7.82 ± 0.03, a pCO_2 maximum of $\sim 652 \pm 6$ µatm and a Ω_A minimum of 0.75 ± 0.16 in the central CB. This pH_T minimum migrates upwards from ~ 180 to ~ 140 meters as the UHL encounters the continental shelf west of M'Clure Strait but maintains its amplitude. The presence of such an acidified layer exacerbates the vulnerability of
315   the planktonic communities in this area, as, in addition to the aragonite undersaturation found at the surface, Ω_A drops below one at depths of 100 to 125 meters or even shallower waters in the Canada Basin. As CO_2 naturally diffuses or mixes from the UHL to the overlying waters and the combination of gas exchange and freshening continues to generate undersaturated conditions at

the surface, the entire photic zone (where $\Omega_A < 1.5$) may acidify and become undersaturated with

320 respect to aragonite at a much faster rate than that of other oceans. The shallowest subsurface aragonite saturation horizon we observe in the central Canada Basin was found at ~85 meters in 2014. Our data do not corroborate the interpretation of Wynn et al. (2016) that the upper boundary of the UHL is migrating downwards due to an expansion of the overlying Polar Mixed Layer (PML), at least not during the period of our observations. The Ω_A crosses the saturation threshold

325 back to supersaturation between 200 and 250 meters, where Atlantic waters become predominant, as evidenced by a +0.8 °C temperature maximum at ~500 m (in contrast to a temperature minimum of -1.5 °C in the UHL). Ω_A and pH_T remain, respectively, above 1.3 and 8.05 in this layer, with respective maxima of 1.74 (± 0.16) and 8.17 (± 0.03) that generally coincide with the temperature maximum mentioned previously. The profiles presented in Fig. 7 do not extend to the bottom of

330 the basin, but deep waters become undersaturated with respect to aragonite below ~2100 m (data from 2009).

The Amundsen Gulf and the western portion of the Parry Channel (Fig. 7; CAA1) essentially exhibit the same water mass structure and carbonate system chemistry as the Canada Basin, as the

335 dominant circulation pattern pushes water eastward from the CB to the CAA. Undersaturation with respect to aragonite does not occur at the surface in these areas, owing to higher salinities. Although the amplitudes of the Ω_A, pH_T and pCO_2 excursions are slightly smaller than those found in the CB, the UHL is considerably shallower in the western CAA. Consequently, Ω_A falls below one at depths of 50 to 70 meters, and the upper portion of the water column in those parts of the

340 CAA might become undersaturated with respect to aragonite even more rapidly than in the CB. As reflected by the blue lines in Fig. 7 (CAA1), the UHL becomes progressively less discernable on depth profiles as it undergoes modification and mixing during its transit from the CB to Lancaster Sound. Atlantic waters are found at the bottom of the water column in the Amundsen Gulf and Parry Channel. The saturation maxima at ~400 m ($\Omega_A \sim 1.1$ to 1.4) are significantly lower

345 in these areas than at similar depths in the CB.

The shallow bathymetry of the central CAA restricts the eastern flow originating from the CB to the layer of Pacific water (UHL) and the overlying surface water. Ω_A is close to 1 at the surface

and reaches a maximum of ~1.45 (± 0.16) at ~30 m, before dipping back below 1 between 50 and
350   75 m, like in other parts of the CAA. With the exception of one profile that exhibits a strong pCO_2
maximum of 685 (± 6.49) µatm as well as pH_T and Ω_A minima of 7.80 (± 0.03) and 0.76 (±0.16),
respectively, at a depth 125 m, this UHL feature becomes less prominent in the central CAA.
Degradation of settling organic matter (remineralization) might explain this exceptional peak of
greater amplitude than those observed in the Canada Basin at Station 310 in September
355   2016.Stratification becomes significantly weaker in the shallow waters (20-100 m) of the Queen
Maud Gulf (Fig. 7; CAA2), one of the areas with the strongest tidal mixing in the CAA
(McLaughlin et al., 2004). The residence time of waters in this area might also be relatively high,
due to its geographical isolation from the main channels of the CAA, possibly allowing more
mixing to take place. The combined effects of low salinities from freshwater accumulation (mostly
360   from river discharge) and the efficient redistribution of CO_2 through mixing result in low carbonate
mineral saturation states throughout the water column. The QMG is the only region in our study
area where the entire water column is undersaturated with respect to aragonite, making it an ideal
location to study the effects of such conditions on aragonitic organisms.

365   East of Barrow Strait, where a sill restricts the eastward flow to the upper 125 meters of the
water column (Bidleman et al., 2007), the water mass regime changes. With the exception of one
profile that captures the Pacific outflow through the western portion of Lancaster Sound at
station 301 (Fig. 7, BB, blue line), this change is clearly visible in profiles of carbonate system
parameters in Lancaster Sound and Baffin Bay, where the upper 500 m of the water column is
370   supersaturated with respect to aragonite at each of the visited stations. Although surface waters
in Northern Baffin Bay are a mixture of multiple inputs from the CAA and the Arctic Ocean
through Nares Strait, the warm and saline Atlantic water inflow from the Labrador Sea
dominates the water-mass structure in the region and accounts for the high alkalinity of these
waters relative to the CB and CAA (Münchow et al., 2015). In Baffin Bay, waters become
375   undersaturated with respect to aragonite and calcite at depths of ~600 and ~1400 meters,
respectively. The pCO_2 and pH_T increase and decrease proportionally to each other with depth.

4.2 Time series

380   Of the 420 stations that make up our dataset, twenty-four were visited at least on two different years and match our comparability criteria for time-series. These criteria are: 1) the stations were sampled within 31 calendar days of each other (this criterion is not ideal since seasonality is highly variable and driven by complex sea-ice processes, including ice break-up) and 2) the stations are located within a 5 km radius. The mean time difference and distance between

385   comparable stations are 12 calendar days and 1.81 km, respectively. Eight were visited three times, the remainder were visited twice. With the exception of one site in northern Baffin Bay, all recurrently sampled stations are located within or on the outskirts of the CAA. Sixteen of the 24 time-series span 3 years or less. Within all comparable stations, we identified the measurements made at similar depths in the top 100 meters of the water column (Fig. 8). The 2014-2015 and

390   2014-2016 intervals have the most comparable data points (~30), followed by the 2007-2009 and 2015-2016 intervals. The remaining year combinations have less than 10 comparable data points. The small data pool applicable to time series and the generally short and inconsistent time intervals between comparable data highlight the poor suitability of our dataset to the identification of temporal trends of ocean acidification. The strong interannual variability of carbonate system

395   parameters in the CAA strengthens this conclusion. Nonetheless, we use data from the seven stations visited over a time interval of at least 5 years (Fig. 9) to identify trends in carbonate system parameters. The resulting depth profiles are shown in Figures 10 and 11.

    To quantify near-surface change, we averaged data from the top 25 meters of the water column. Across this depth interval, between 2007 and 2016, the temperature-normalized pCO_2,

400   DIC and DIC/TA at site LS1 rose by 36 ± 9 µatm, 37 ± 10 µmol kg^{-1} and 0.008 ± 0.005, while pH_T and Ω_A decreased by 0.042 ± 0.037 and 0.12 ± 0.23, respectively. Given its uncertainty, the change in Ω_A is insignificant. The same trend is visible between the same years at station CAA1, at a greater magnitude (+ 78 µatm pCO_2, -0.088 pH_T unit, -0.37 Ω_A unit), except for a DIC decrease of 58 µmol kg^{-1} caused by a decrease in salinity of 1.76. The DIC/TA, which effectively normalizes

405   DIC against salinity, shows an increase of 0.021, proportional to the change in the other parameters. Data from the nearby station CAA2 also displays a similar trend between 2009 and 2015 (+ 29 µatm pCO_2, -0.041 pH_T unit, +0.001 DIC/TA), albeit a strong positive change in

Biogeosciences
Discussions

salinity (+1.81) contributed to an increase of 0.06 Ω_A unit (again, insignificant given its uncertainty of 0.23).

410

Four stations located on the transect extending from Cape Bathurst to Banks Island complete the seven time-series of at least five years (Fig. 11). Three of those time series (AM1, AM2, AM4) span 2003-2009 or 2004-2009. Thus, given their spatial and temporal proximity, we expect a certain consistency in the trends they exhibit. Surprisingly, salinity increased at each of the stations, by 1.46, 0.70 and 0.13, respectively. Despite the consistent salinity trend, stations AM2 and AM4 show opposite trends in carbonate system parameters, the former exhibiting a positive change in pCO_2 (+ 49 ± 9 µatm) and DIC/TA (+ 0.010 ± 0.005) as well as a negative change in pH_T (-0.089 ± 0.037) and Ω_A (-0.20 ± 0.23), while the latter displays negative but somewhat smaller changes in pCO_2 (- 35 ± 9 µatm) and DIC/TA (- 0.007 ± 0.005) as well as a positive change in pH_T (+0.051 ± 0.037) and Ω_A (+0.13 ± 0.23), mostly apparent near the surface (<10 m). The two profiles recorded at site AM2 exhibit a clear difference in stratification; a sharp peak in carbonate system parameters (associated with a temperature maximum) appears at ~25 m in 2003, while the top 50 meters were fairly uniform in terms of pCO_2, pH_T and DIC/TA in 2009. The magnitude of change in the carbonate system parameters at stations AM1 (2004-2009) and AM3 (2009-2016) is below their respective uncertainties. A relatively large change of -1.90 in near-surface salinity is observable at station AM3. The depth profiles at sites AM1 and AM3 (Fig. 11), both of which include measurements from three separate years, highlight the non-linearity of change (i.e., the variation between the earliest and the intermediate year is opposite from the variation between the earliest and latest years). Although this observation is limited to two groups of profiles, it constitutes a caveat to conclusions drawn from only two points in time.

Below 25 meters depth, variations in atmospheric conditions and biological activity become decreasingly influential on carbonate system parameters, relative to changes in water mass properties resulting from mixing. The largest change in our time series occurs at Station LS1, where pCO_2, DIC and DIC/TA increased by 265 µatm, 95 µmol kg^{-1}, and 0.040, and pH_T and Ω_A decreased by 0.140 and 0.38, respectively, over the 25-100 m depth interval, between 2007 and 2016. This drastic change reflects the varying proportions of Pacific and Atlantic Ocean waters

that reach Lancaster Sound, the latter water mass intruding episodically into the CAA (Prinsenberg and Bennett, 1987). An increase in the abundance (or a change in the properties) of Pacific Ocean

440   water between 2007 and 2016 is likely the cause of this feature, as a similar trend is visible at station CAA1, located east of Barrow Strait, where the intrusion of Atlantic Ocean water is halted by a 125-m sill. This is supported by the absence of a strong increase in salinity in Lancaster Sound in 2007, which could be interpreted as a pulse of intruding Atlantic Ocean water. This feature is reversed at station CAA2 between 2009 and 2015, highlighting the interannual variability in the

445   properties of the UHL. Below this layer, water properties are relatively uniform in time at stations CAA1, CAA2, LS1 and AM2, except for pCO_2 variations on the order of 20 to 30 μatm. Station AM1 exhibits a strong change in deep-water (300 to 400 m) properties between 2004 and 2008, the latter year displaying considerably less acidic conditions (+ 0.25 pH_T unit), while salinity and temperature profiles are nearly identical for the two years, suggesting vertical carbon export from

450   the surface as a possible mechanism.

As previously stated, these time series are snapshots in time and cannot be assumed to represent the continuous evolution of the carbonate chemistry in the Canadian Arctic. Nonetheless, even with a small sample size, we can confidently state that the temporal evolution of carbonate

455   system parameters in the region does not display a systematic trend on sub-decadal timescales. Moreover, most of the significant changes our time series exhibit are associated to variations in the physical oceanography of the region (water-mass distribution and circulation) or surface processes (melting of sea-ice). Given the well-documented rapid melting of the sea-ice cover in the region (e.g., Tivy et al., 2011), we did not expect to observe increases in summer surface

460   salinity over time intervals of 5 to 9 years. Our time series, therefore, offer proof of the strong interannual variability of this highly dynamic system. Discerning the ocean acidification signal amid the various physical and biological sources of change would require continuous time series over a longer period of time. We estimated this period to 23 to 35 years for pH, 25 to 37 years for pCO2, 31 to 46 for ΩA and 118 to 177 years for DIC using calculations of Time of Emergence, or

465   the time required for the effects of a process to emerge from the natural variability of a system (see Appendix A). Time of emergence calculations are usually performed with large, continuous datasets from climate models; we therefore do not consider these results to be statistically correct.

Nonetheless, this exercise shows the relative variabilities of the carbonate system parameters and highlights the particularly strong variability of DIC, which is the object of the next section. Its
470   results also imply that without accurate measurements of the effects of biological activity and sea-ice processes (both major drivers of natural variability), direct detection of the ocean acidification signal will require at least 20-25 years of observations. Gathering data in the CAA in the next few years is therefore critical, as regular ship-based observational campaigns in the region started in the early 2000's (Giesbrecht et al., 2014).

475

4.3 The biological contribution to interannual DIC variations: ΔDIC_{Bio}

We define ΔDIC_{Bio} as the change in the contribution of in-situ biological activity (photosynthesis and respiration) to the DIC of a parcel of water over a given period of time. ΔDIC_{Bio} is calculated for each depth at recurrently visited stations according to:

480
$$\Delta DIC_{BIO} = DIC_{Observed} - DIC_{Reference}$$

where $DIC_{Reference}$ is computed in CO2SYS using the temperature-normalized seawater pCO_2 calculated at a reference time (from measured TA and pH_T) and the TA measured at the time of interest (the year for which ΔDIC_{Bio} is reported). The change in global mean atmospheric CO_2 concentrations between the reference year and the year of interest is added to the pCO_2 in order to
485   account for gas exchange (data from Dlugokencky and Tans, NOAA/ESRL). This approximation rests on the assumption that the yearly increase in surface water pCO_2 follows that of the atmosphere (given stable biological production), as observations from global monitoring stations demonstrate (e.g., González-Dávila et al., 2010), although the validity of this claim is weakened on short spatial and temporal (sub-decadal) scales (Fay et al., 2013, Wanninkhof et al., 2013). This
490   also restricts our calculations to the upper portion of the water column (25 m) that is in direct contact with the atmosphere. Under the additional assumptions that DIC is only affected by gas exchange, biological activity and mixing, and that TA is not significantly affected by biological activity (Zeebe and Wolf-Gladrow, 2001), $DIC_{Reference}$ represents the DIC of a parcel of water if its *in-situ* biological component remained unchanged relative to a reference year (i.e., identical
495   contribution, negative or positive, from the balance between photosynthesis and respiration). Because the reference pCO_2 is calculated in part from TA, changes in water masses should not

affect the results of this analysis, given the salinity range of the data subset used in the calculation of ΔDIC_{Bio} ($25.6 < S_P < 33.7$). Thus, ΔDIC_{Bio} can provide insights into the interannual variability of biological activity in the Canadian Arctic, without direct measurements of parameters such as chlorophyll or biomass.

Figure 12 shows ΔDIC_{Bio}, averaged over the top 25 meters of the water column, at the 18 stations where comparable data were available, all located in the Amundsen Gulf and CAA. The magnitude of the calculated ΔDIC_{Bio} is beyond its uncertainty, which varies from 6.4 to 14.3 µmol kg^{-1} (mean of $\pm$ 8.6 µmol kg^{-1}), at 11 locations out of 18. All significant results from the month of October (2003-2009 and 2007-2009) in the Amundsen Gulf show a positive mean ΔDIC_{Bio} (a decrease in biological DIC uptake and/or an increase in DIC production) of up to 20.6 ± 10.5 µmol kg^{-1}. Conversely, the ΔDIC_{Bio} calculated for the month of August (2004-2009, 2009-2016 and 2014-2015) is generally negative and of a similar magnitude. Data for September are variable in direction and show the greatest change over consecutive years: relative to 2014, in the Amundsen Gulf, the mean ΔDIC_{Bio} fluctuated in 2015 and 2016 by $+28.0 \pm 11.0$ to -11.2 ± 8.0 µmol kg^{-1} over the 0-25 m depth interval.

It is unlikely that the consistent directions of change we observe for the months of August and October represent actual trends, given the small data pool and inconsistent reference states used to make those observations. Nevertheless, we can use this analysis to constrain the contribution of fluctuations in biological activity to the interannual variability of the DIC. In the top 25 meters of the water column, the maximum amplitude of ΔDIC_{Bio} is 45.9 ± 11.5 µmol kg^{-1}, observed in the Amundsen Gulf between 2014 and 2015. This maximum is not visible on Fig. 14, which only shows mean values. The Pearson correlation coefficient (r) between ΔDIC_{Bio} and ΔDIC (the change in DIC over the same time interval) is 0.52 and the associated coefficient of determination (R^2) is 0.27, suggesting that 27% of the interannual variability in surface DIC in the Canadian Arctic Archipelago is a direct result of the variability in biological activity. This has important implications with respect to the interpretation of DIC time series in the region and explains, in part, the long time of emergence of DIC as a proxy for acidification, compared to other carbonate system parameters, as hypothesized in section 4.2.

The extremely weak (r = 0.08) correlation between ΔDIC_{Bio} and the time interval over which it applies provides additional evidence of the absence of a trend in the balance between photosynthesis and respiration in the surface waters of the Canadian Arctic. The variability in this balance is driven by many interconnected, often localized processes. For instance, short-lived episodes of upwelling of halocline waters not only directly change the chemical properties at the surface, but also provide nutrients that stimulate biological activity (Tremblay et al., 2011). Primary production in the Arctic is also closely linked to the seasonal cycle of sea-ice (e.g., Arrigo et al., 2008). Beyond its natural fluctuations, ongoing disruptions to this cycle and other physical properties (stratification, temperature, etc.) forced by climate change are known to affect phytoplankton communities and their productivity (Ardyna et al., 2014; Blais et al., 2017), possibly increasing their imprint on the variability of DIC and other carbonate system parameters. As previously mentioned, variations in water mass composition cannot directly explain variations in ΔDIC_{Bio}. Nonetheless, mixing is likely accompanied by changing nutrient concentrations, which influence the balance of photosynthesis and respiration (Tremblay et al., 2015).

5 Conclusions

Field observations of carbonate system parameters made between 2014 and 2016 in the Canadian Arctic reveal that surface waters of the region serve as a net CO_2 sink in the summer and are generally close to saturation with respect to aragonite ($1 < \Omega_A < 1.5$). Surface undersaturation ($\Omega_A < 1.0$) is found predominantly in the central Canada Basin, as documented in previous years (Yamamoto-Kawai et al., 2011; Robbins et al., 2013), and in the freshwater-influenced Queen Maud Gulf, the only area of the Canadian Arctic where the entire water column is undersaturated with respect to aragonite. The CO_2 – rich Upper Halocline Layer is the locus of shallow aragonite undersaturation horizon at depths of 85 to 125 m in the Canada Basin and 50 to 70 m in the Canadian Arctic Archipelago, further fostering undersaturation near the surface and potentially threatening marine calcifying organisms living in this portion of the water column.

555   Time series of carbonate system parameters, although relatively short (<10 years) and incomplete, illustrate the strong interannual variability of the region, due in part to complex circulation patterns and varied water mass assemblages. Our estimates of ΔDIC_{BIO}, the change in the contribution of biological activity to DIC, suggest that variations in biological activity (the balance between photosynthesis and respiration) account for approximately a third of the

560   interannual variability of DIC measurements. Additional work must also be carried out to extend this estimate to other carbonate system parameters (pH, pCO_2, Ω). In order to test the validity of the ΔDIC_{BIO} concept and its underlying assumptions, our results should be compared to direct measurements of biological productivity (e.g. biomass, chlorophyll-a) during the same time period. Without the latter, the quantification of the progression of ocean acidification in the surface waters

565   of the Canadian Arctic will require longer and more continuous time series, the length of which can be estimated using the concept of Time of Emergence. Future work on ocean acidification in this region should focus on obtaining continuous time series of carbonate system parameters, especially in areas where surface waters might soon become undersaturated with respect to aragonite, as well as bridging the gap between observations of carbonate mineral saturation and

570   markers of ecosystem heath.

575

580

Appendix A

Time of Emergence of ocean acidification signals

The time of emergence (ToE) of a process affecting a natural system is the time required for the measurable effects of this process to emerge from the natural variability of the system. The concept is predominantly applied in global climate change modeling studies, for which the results are either "years of emergence" based on a pre-industrial steady-state (e.g., Friedrich et al., 2012) or time intervals over which observations must be made in order to distinguish an anthropogenic signal from natural variability. Few of these studies have used observations (e.g., Sutton et al. 2016), and, to our knowledge, none of them have focused specifically on the Arctic.

We define the time of emergence according to the following equation:

(A1)
$$ToE = \frac{C \times N}{S}$$

in which N is the natural variability, defined (after Hawkins and Sutton, 2012) as the standard deviation of the annual means of one of four parameters (DIC, T-normalized pCO_2, Ω_A, pH_T), across 7 years from 2003 to 2016. S is the slope (in units per year) of the theoretical acidification curve, constructed by calculating the evolution of a given parameter in CO2SYS, at a constant alkalinity (2000 µmol kg^{-1}), practical salinity (30) and temperature (0°C), and assuming that the surface ocean pCO_2 increases at the same mean rate as the atmospheric pCO_2 between 2003 and 2016 (data from Dlugokencky and Tans, NOAA/ESRL). Our computed rates of acidification (Table A1) are in general agreement with the values reported by Bates et al. (2014). C is a constant that sets the threshold of emergence at either 2 or 3 standard deviations (N), i.e., when the acidification signal becomes significant beyond natural variability as it emerges from 95% or 99.7% of the observed annual mean values, assuming the data (or the naturally occurring values of the parameter they represent) are normally distributed. Only data collected from June to October, inclusively, are used to minimize the effect of seasonal variability.

605

Biogeosciences
Discussions

Although the assumption of relative equilibration with atmospheric pCO_2 might be less applicable at these depths, we applied the same technique using data from depths of 100 m and 300 m in order to estimate the time of emergence below the surface, where the interannual variability should be relatively small. Significant acidification at these depths might be due in large part to advection

610 (e.g., Luo et al., 2016) rather than gas exchange.

The results of this analysis are presented in Table A2. At the surface, pH_T and pCO_2 have very similar times of emergence of 23-35 years and 25-37 years for C values of 2 and 3, respectively. The Ω_A signal emerges after a slightly longer time, 31-46 years. The ToE of DIC is

615 considerably longer than that of the three other parameters, at 118-177 years. The discrepancy between DIC and the other parameters is largely due to chemical considerations, as the high Revelle factors (15-20) in the region imply that the change in pCO_2 caused by the uptake of atmospheric CO_2 will be 15 to 20 times larger than that of DIC, relative to their initial concentrations.

620 Our results show a slight increase of ToE values from the surface to the 90-110 m depth interval (except for Ω_A that remains identical), followed by a decrease below surface values at the 290-310 m depth interval (except for DIC). We attribute the relatively strong variability of the ToE in the 90-110 m depth interval to a periodical vertical migration of the upper boundary of the metabolic CO_2-rich (low pH_T, Ω_A, high pCO_2, DIC) Upper Halocline Layer (UHL) that is found

625 at depths of ~100-200 m throughout most of the study area. The results are also likely affected by the decreasing number of data with depth (Table A3), that could lead to less accurate annual means and explain the increase of the DIC ToE from the surface to the 290-310 m interval.

Despite their similarity, our calculated times of emergence are consistently longer than

630 those reported in modelling studies (Keller et al., 2014; Rodgers et al., 2015) This is consistent with the fact that coastal waters, that comprise a large portion of our dataset, exhibit a much higher variability in pH (and other carbonate system parameters) than open oceans (Duarte et al. 2013). Furthermore, direct observations are likely to integrate variability on temporal and spatial scales that are too small to be resolved by models. It is also important to note that distinct measurement

635   techniques and their associated uncertainties create an analytical bias between different parameters, a bias that is not present in the same form in modelling studies. The relative uncertainties of *in-situ* pH_T (0.3%) measurements as well as computed pCO_2 (4.5%) and Ω_A (6.4%) values are strongly correlated with their increasing times of emergence in the 0-25 m depth interval (r=0.88). Although this correlation becomes significantly weaker (r=0.49) when DIC and its

640   relative uncertainty (0.4%) are included in the analysis, it suggests the presence of an analytical bias in our ToE estimates. Nonetheless, the similarity between the ToE of pH_T and pCO_2 as well as the large ToE of DIC are consistent with the findings of Keller et al. (2014).

        The validity of these conclusions depends on a methodology that differs considerably from its

645   modelling equivalent, even if the results from both approaches are consistent with each other. In addition to the instrumental bias mentioned previously, our observations are subject to a sampling bias, since we only use data gathered in the summer months. Consequently, the natural variability used in our TOE calculations does not encompass the entire annual cycle. Nevertheless, because we define the natural variability of the system in terms of interannual rather than seasonal changes,

650   the former should not change, assuming the amplitude of the seasonal cycle is constant through time. The other form of sampling bias possibly affecting our results is spatial, as cruise tracks and durations varied every summer.

        Appendix B

655   **Estimation of the freshwater sources in the Queen Maud Gulf**

        In order to estimate the relative fractions of sea-ice melt and meteoric water (mostly river water) in the Queen Maud Gulf, we use $\delta^{18}O$ and practical salinity (S_P) data collected in the area in 2015 to perform a linear regression analysis. The methods of analysis of the oxygen isotopes, reported on the $\delta^{18}O$ notation (V-SMOW), are described in detail in Lansard et al. (2012) for the samples

660   collected during the CASES expedition (2003-2004) and in Mucci et al. (2018) for the remainder of the samples.

Using the intercept of the trendline equation ($\delta^{18}O = 0.5282S_P - 18.552$) to extrapolate $\delta^{18}O$ to S_P = 0, we find the mean $\delta^{18}O$ of the freshwater found in the Queen Maud Gulf in 2015 to be -18.55 ‰. Based on the $\delta^{18}O$ values of meteoric water (-18.9 ± 0.1 ‰) and sea-ice melt (-2.0 ± 0.5 ‰)

665   used by Lansard et al. (2012), the fractions of meteoric (river) water and sea-ice melt would be, respectively, 98% and 2%. A potential source of error affecting this estimate is the use of the $\delta^{18}O$ of Mackenzie River water as the riverine end-member, which might differ significantly from the oxygen isotope signature of the rivers discharging in the Queen Maud Gulf.

670   **Data availability**

The raw data collected as a part of the ArcticNet program, on which most of the observations presented in this paper are based can be accessed through the Polar Data Catalogue (Mucci, 2017). Complementary datasets, some of which are part of larger databases, are also available on various online repositories (François et al., 2012; Chierici et al., 2013; Giesbrecht et al., 2014;

675   Papakyriakou et al., 2017).

Author contribution

A.M. and A. B.-L. conceived the project. A.M. and H.T. acquired much of the data prior to 2016. A. B.-L. carried out the data analysis and wrote the first draft of the paper whereas A.M. and H. T.

680   provided editorial and scientific recommendations. H.T. provided results of alkalinity and dissolved inorganic carbon analyses and scientific recommendations.

Competing interests

The authors declare that they have no conflict of interest.

685

Biogeosciences
Discussions

Open Access

EGU

6 References

Ahmed, M., Else, B. G. T., Burgers, T. M. and Papakyriakou, T.: Variability of surface water pCO_2
in the Canadian Arctic Archipelago from 2010 to 2016, J. Geophys. Res. Oceans, 124,
doi:10.1029/2018JC014639, 2019.

Ardyna, M., Babin, M., Gosselin, M., Devred, E., Rainville, L. and Tremblay, J.: Recent Arctic
Ocean sea ice loss triggers novel fall phytoplankton blooms, Geophys. Res. Lett., 41, 6207-6212,
doi:10.1002/2014GL061047, 2014.

Arrigo, K. R., van Dijken, G. and Pabi, S.: Impact of a shrinking Arctic ice cover on marine
primary production, Geophys. Res. Lett., 35, L19603, doi:10.1029/2008GL035028, 2008.

Bates, N. R., Astor, Y. M., Church, M. J., Currie, K., Dore, J. E., Gonzalez-Davila, M., Lorenzoni,
L., Muller-Karger, F., Olafsson, J. and Santana-Casiano, J. M.: A time-series view of changing

715   surface ocean chemistry due to ocean uptake of anthropogenic CO_2 and ocean acidification, Oceanography, 27, 126-141, doi:10.5670/oceanog.2014.16, 2014.

Bidleman, T.F., Kylin, H., Jantunen, L. M., Helm, P. A. and MacDonald, R. W.: Hexachlorocyclohexanes in the Canadian archipelago. spatial distribution and pathways of α-, β- and γ-HCHs in surface water., Environmental Science and Technology, 41, 2688-95, 2007.

720   Blais, M., Ardyna, M., Gosselin, M., Dumont, D., Belanger, S., Tremblay, J., Gratton, Y., Marchese, C. and Poulin, M.: Contrasting interannual changes in phytoplankton productivity and community structure in the coastal Canadian Arctic Ocean, Limnol. Oceanogr., 62, 2480-2497, doi:10.1002/lno.10581, 2017.

Bopp L., Resplandy, L., Orr, J. C., Doney, S. C. and Dunne, J. P.: Multiple stressors of ocean
725   ecosystems in the 21st century: projections with CMIP5 models, Biogeosciences, 10, 6225-6245, 2013.

Bourke, R., Addison, V. and Paquette, R.: Oceanography of Nares Strait and Northern Baffin-Bay in 1986 with emphasis on deep and bottom water formation, J. Geophys. Res.: Oceans, 94, 8289-8302, doi:10.1029/JC094iC06p08289, 1989.

730   Brunskill, G. J.: Environmental features of the Mackenzie system, in: The ecology of river systems. Junk Publishers, Dordrecht, Netherlands, 435-471, 1986.

Carmack, E.C. and MacDonald, R.: Oceanography of the Canadian shelf of the Beaufort Sea: A setting for marine life, Arctic, 55, 29-45, 2002.

Carmack, E.C., Macdonald, R. and Papadakis, J.: Water mass structure and boundaries in the
735   Mackenzie Shelf estuary, Journal of Geophysical Research: Oceans, 94, 18043-18055, 1989.

Chierici, M. and Fransson, A.: Calcium carbonate saturation in the surface water of the Arctic Ocean: Undersaturation in freshwater influenced shelves, Biogeosciences, 6, 2421-2431, doi:10.5194/bg-6-2421-2009, 2009.

Chierichi, M. and Thomas, H.: CO2 system data during the Circumpolar Flaw Lead, Polar Data
740   Catalogue, www.polardata.ca/pdcsearch/PDCSearchDOI.jsp?doi_id=10900, 2013.

Clayton, T. and Byrne, R.: Spectrophotometric seawater pH measurements - total hydrogen-ion concentration scale calibration of M-Cresol Purple and at-sea results, Deep-Sea Res. Part I- Oceanogr. Res. Pap., 40, 2115-2129, doi:10.1016/0967-0637(93)90048-8, 1993.

Dery, S.J., Stadnyk, T. A., MacDonald, M. K. and Gauli-Sharma, B.: Recent trends and variability
745   in river discharge across northern Canada, Hydrology and Earth System Sciences, 20, 4801-4818, doi:10.5194/hess-20-4801-2016, 2016.

Dickson, A. G.: Standard potential of the reaction - AgCl(s)+1/2H$_2$(g)=Ag(s)+HCl(aq) and the standard acidity constant of the ion HSO$_4^-$ in synthetic sea-water from 273.15K to 318.15K, J. Chem. Thermodyn., 22, 113-127, doi:10.1016/0021-9614(90)90074-Z, 1990.

750   Dickson, A. G. and Millero, F.: A comparison of the equilibrium-constants for the dissociation of carbonic-acid in seawater media, Deep-Sea Research Part A-Oceanographic Research Papers, 34, 1733-1743, doi:10.1016/0198-0149(87)90021-5, 1987.

Dickson, A. G., Sabine, C. L., and Christian, J. R.: Guide to best practices for ocean CO$_2$ measurements PICES Special Publications, 191 pp., 2007.

755   Dlugokencky, E. and Tans, P.: Trends in atmospheric carbon dioxide, National Oceanic & Atmospheric Administration, Earth System Research Laboratory (NOAA/ESRL), available at: http: //www.esrl.noaa.gov/gmd/ccgg/trends/global.html.

Duarte, C. M., Hendriks, I. E., Moore, T. S., Olsen, Y. S., Steckbauer, A., Ramajo, L., Carstensen, J., Trotter, J. A. and McCulloch, M.: Is ocean acidification an open-ocean syndrome?
760   Understanding anthropogenic impacts on seawater pH, Estuaries Coasts, 36, 221-236, doi:10.1007/s12237-013-9594-3, 2013.

Emmerton, C. A., Lesack, L. F. W. and Vincent, W. F.: Nutrient and organic matter patterns across the Mackenzie River, estuary and shelf during the seasonal recession of sea-ice, J. Mar. Syst., 74, 741-755, doi:10.1016/j.jmarsys.2007.10.001, 2008.

765   Fay, A. R. and G. A. McKinley, G. A.: Global trends in surface ocean pCO$_2$ from in situ data, Global Biogeochem. Cycles, 27, 541–557, doi:10.1002/gbc.20051, 2013.

Francois, R., Mucci, A., Holmden, C., Varela D., Cullen, J., Orians, K., Maldonado, M., Tortell, P., Rivkin, R., Kienast, M., Thomas, H., Hale, M., Miller, L., Smith, J.N., Sigman, D., Brzezinski, M., Weis, D., Fones, G., Saito, M., Allen, A., and Williamson, S.: GEOTRACES: Multi-tracer
770   investigation of the effect of climate change on nutrient and carbon cycles in the Arctic Ocean, Canadian Cryospheric Information Network (CCIN), http://dx.doi.org/10.5443/11458, 2012.

Friedrich, T., Timmermann, A., Abe-Ouchi, A., Bates, N. R., Chikamoto, M. O., Church, M. J., Dore, J. E., Gledhill, D. K., Gonzalez-Davila, M., Heinemann, M., Ilyina, T., Jungclaus, J. H., McLeod, E., Mouchet, A. and Santana-Casiano, J. M.: Detecting regional anthropogenic trends in
775   ocean acidification against natural variability, Nat. Clim. Chang., 2, 167-171, doi:10.1038/NCLIMATE1372, 2012.

Geilfus, N.X., Pind, M. L., Else, B. G. T., Galley, R. J., Miller, L. A., Thomas, H., Gosselin, M., Rysgaard, S., Wang, F. and Papakyriakou, T. N.: Spatial and temporal variability of seawater pCO$_2$ within the Canadian Arctic Archipelago and Baffin Bay during the summer and autumn 2011,
780   Cont. Shelf Res., 156, 1-10, doi:10.1016/j.csr.2018.01.006, 2018.

Giesbrecht, K. E., Miller, L. A., Davelaar, M., Zimmermann, S., Carmack, E., Johnson, W. K., Macdonald, R. W., McLaughlin, F., Mucci, A., Williams, W. J., Wong, C. S. and Yamamoto-

Kawai, M.: Measurements of the dissolved inorganic carbon system and associated biogeochemical parameters in the Canadian Arctic, 1974-2009, Earth System Science Data, 6, 91-104, doi:10.5194/essd-6-91-2014, 2014.

785

Gonzalez-Davila, M., Santana-Casiano, J. M., Rueda, M. J. and Llinas, O.: The water column distribution of carbonate system variables at the ESTOC site from 1995 to 2004, Biogeosciences, 7, 3067-3081, doi:10.5194/bg-7-3067-2010, 2010.

Hawkins, E. and Sutton, R.: Time of emergence of climate signals, Geophys. Res. Lett., 39, L01702, doi:10.1029/2011GL050087, 2012.

790

Iseki K., Macdonald R.W. and Carmack E.C.: Distribution of particulate matter in the southeastern Beaufort Sea in late summer. Proc. NIPR Symp. Polar. Biol. 1:35–46, 1987.

Jiang, L., Cai, W. and Wang, Y.: A comparative study of carbon dioxide degassing in river- and marine-dominated estuaries, Limnol. Oceanogr., 53, 2603-2615, doi:10.4319/lo.2008.53.6.2603, 2008.

795

Johnson, K., Wills, K., Butler, D., Johnson, W. and Wong, C.: Coulometric total carbon-dioxide analysis for marine studies - maximizing the performance of an automated gas extraction system and coulometric detector, Mar. Chem., 44, 167-187, doi:10.1016/0304-4203(93)90201-X, 1993.

Jones, E., Anderson, L. and Swift, J.: Distribution of Atlantic and Pacific waters in the upper Arctic Ocean: Implications for circulation, Geophys. Res. Lett., 25, 765-768, doi:10.1029/98GL00464, 1998.

800

Jones, E., Swift, J., Anderson, L., Lipizer, M., Civitarese, G., Falkner, K., Kattner, G. and McLaughlin, F.: Tracing Pacific water in the North Atlantic Ocean, J. Geophys. Res. -Oceans, 108, 3116, doi:10.1029/2001JC001141, 2003.

805 Keller, K. M., Joos, F. and Raible, C. C.: Time of emergence of trends in ocean biogeochemistry, Biogeosciences, 11, 3647-3659, doi:10.5194/bg-11-3647-2014, 2014.

Lansard, B., Mucci, A., Miller, L. A., Macdonald, R. W. and Gratton, Y.: Seasonal variability of water mass distribution in the southeastern Beaufort Sea determined by total alkalinity and delta O-18, Journal of Geophysical Research.Oceans, 117, 2012.

810 Le Quere, C., Andrew, R. M., Friedlingstein, P., Sitch, S., Pongratz, J., Manning, A. C., Korsbakken, J. I., Peters, G. P., Canadell, J. G., Jackson, R. B., Boden, T. A., Tans, P. P., Andrews, O. D., Arora, V. K., Bakker, D. C. E., Barbero, L., Becker, M., Betts, R. A., Bopp, L., Chevallier, F., Chini, L. P., Ciais, P., Cosca, C. E., Cross, J., Currie, K., Gasser, T., Harris, I., Hauck, J., Haverd, V., Houghton, R. A., Hunt, C. W., Hurtt, G., Ilyina, T., Jain, A. K., Kato, E., Kautz, M., 815 Keeling, R. F., Goldewijk, K. K., Koertzinger, A., Landschuetzer, P., Lefevre, N., Lenton, A., Lienert, S., Lima, I., Lombardozzi, D., Metzl, N., Millero, F., Monteiro, P. M. S., Munro, D. R., Nabel, J. E. M. S., Nakaoka, S., Nojiri, Y., Padin, X. A., Peregon, A., Pfeil, B., Pierrot, D., Poulter, B., Rehder, G., Reimer, J., Roedenbeck, C., Schwinger, J., Seferian, R., Skjelvan, I., Stocker, B.

820   D., Tian, H., Tilbrook, B., Tubiello, F. N., van der Laan-Luijkx, I. T., van der Werf, G. R., van
       Heuven, S., Viovy, N., Vuichard, N., Walker, A. P., Watson, A. J., Wiltshire, A. J., Zaehle, S. and
       Zhu, D.: Global Carbon Budget 2017, Earth Syst. Sci. Data, 10, 405-448, doi:10.5194/essd-10-
       405-2018, 2018.

       Lewis, E. and Wallace, D.W.R.: Program developed for CO_2 system calculations. Carbon Dioxide
       Information Analysis Center, Oak Ridge National Laboratory, US Department of Energy, Oak
825   Ridge, Tennessee, 1998.

       Luo, Y., Boudreau, B. P. and Mucci, A.: Disparate acidification and calcium carbonate
       desaturation of deep and shallow waters of the Arctic Ocean, Nat. Commun., 7, 12821,
       doi:10.1038/ncomms12821, 2016.

       Macdonald, R.W., Carmack, E., McLaughlin, F., Iseki, K. and Macdonald, D.: Composition and
830   modification of water masses in the Mackenzie Shelf estuary, Journal of Geophysical Research:
       Oceans, 94, 18057-18070, 1989.

       Macdonald, R. and Yu, Y.: The Mackenzie estuary of the Arctic Ocean, in: The Handbook of
       Environmental Chemistry, vol. 5H. Springer, Berlin/Heidelberg, 91-120, 2006.

       McLaughlin, F. A., Carmack, E. C., Ingram, R. G., Williams, W. J. and Michel, C.: Oceanography
835   of the Northwest Passage, in: The Sea, Vol. 14. Wiley, New York, 1121-1242, 2004.

       Mehrbach, C., Culberson, C.H., Hawley, J.E. and Pytkowicz, R.M.: Measurement of the apparent
       dissociation constants of carbonic acid in seawater at atmospheric pressure. Limnol. Oceanogr. 18,
       897 – 907, 1973.

       Melling, H., Gratton, Y. and Ingram, G.: Ocean circulation within the North Water Polynya of
840   Baffin Bay, Atmosphere-Ocean, 39, 301-325, doi:10.1080/07055900.2001.9649683, 2001.

       Miller, L. A., Papakyriakou, T. N., Collins, R. E., Deming, J. W., Ehn, J. K., Macdonald, R. W.,
       Mucci, A., Owens, O., Raudsepp, M. and Sutherland, N.: Carbon dynamics in sea ice: A winter
       flux time series, J. Geophys. Res. -Oceans, 116, C02028, doi:10.1029/2009JC006058, 2011.

       Millero, F. J.: Chemical Oceanography, 3rd Edn., CRC Press, Boca Raton, Florida, 2005.

845   Mostofa, K. M. G., Liu, C., Zhai, W., Minella, M., Vione, D., Gao, K., Minakata, D., Arakaki, T.,
       Yoshioka, T., Hayakawa, K., Konohira, E., Tanoue, E., Akhand, A., Chanda, A., Wang, B. and
       Sakugawa, H.: Reviews and syntheses: Ocean acidification and its potential impacts on marine
       ecosystems, Biogeosciences, 13, 1767-1786, doi:10.5194/bg-13-1767-2016, 2016.

       Mucci, A.: The Solubility of calcite and aragonite in seawater at various salinities, temperatures,
850   and one atmosphere total pressure, Am. J. Sci., 283, 780-799, doi:10.2475/ajs.283.7.780, 1983.

Biogeosciences
Discussions

EGU

Mucci, A., Lansard, B., Miller, L. A. and Papakyriakou, T. N.: CO_2 fluxes across the air-sea interface in the southeastern Beaufort Sea: Ice-free period, J. Geophys. Res. -Oceans, 115, C04003, doi:10.1029/2009JC005330, 2010.

855   Mucci, A.: Long-term Monitoring of pH, total alkalinity, the stable oxygen isotopic composition of water and the stable carbon isotopic composition of dissolved inorganic carbon in the Canadian Arctic. Waterloo, Canada: Canadian Cryospheric Information Network (CCIN). http://dx.doi.org/10.5884/12733, 2017

Mucci, A., Levasseur, M., Gratton, Y., Martias, C., Scarratt, M., Gilbert, D., Tremblay, J., Ferreyra, G. and Lansard, B.: Tidally induced variations of pH at the head of the Laurentian
860   Channel, Can. J. Fish. Aquat. Sci., 75, 1128-1141, 10.1139/cjfas-2017-0007, 2018.

Muench. R.D.: The physical oceanography of the northern Baffin Bay Region. North Water Project Scientific Report No. 1, Arctic Institute of North America, 150 pp., 1971.

Munchow, A., Falkner, K. K. and Melling, H.: Baffin Island and West Greenland current systems in northern Baffin Bay, Prog. Oceanogr., 132, 305-317, 2015.

865   Orr, J. C., Epitalon, J., Dickson, A. G. and Gattuso, J.: Routine uncertainty propagation for the marine carbon dioxide system, Mar. Chem., 207, 84-107, doi:10.1016/j.marchem.2018.10.006, 2018.

Orr, J., Fabry, V., Aumont, O., Bopp, L., Doney, S., Feely, R., Gnanadesikan, A., Gruber, N., Ishida, A., Joos, F., Key, R., Lindsay, K., Maier-Reimer, E., Matear, R., Monfray, P., Mouchet,
870   A., Najjar, R., Plattner, G., Rodgers, K., Sabine, C., Sarmiento, J., Schlitzer, R., Slater, R., Totterdell, I., Weirig, M., Yamanaka, Y. and Yool, A.: Anthropogenic ocean acidification over the twenty-first century and its impact on calcifying organisms, Nature, 437, 681-686, doi:10.1038/nature04095, 2005.

Papakyriakou, T., Miller, L. A., Thomas, H.,; Mucci, A. and Else, B.: Partial pressure of carbon
875   dioxide, dissolved inorganic carbon, alkalinity, temperature, salinity and other variables collected from the surface underway observations and discrete bottle samples from CCGS Amundsen during the cruises in Baffin Bay, Nares Strait, and Lancaster Sound from 2013-08-11 to 2014-08-12,. NOAA National Centers for Environmental Information, https://doi.org/10.7289/v5st7n3c. 2017.

880   Popova, E. E., Yool, A., Aksenov, Y., Coward, A. C. and Anderson, T. R.: Regional variability of acidification in the Arctic: a sea of contrasts, Biogeosciences, 11, 293-308, doi:10.5194/bg-11-293-2014, 2014.

Prinsenberg, S. and Bennett, E.: Mixing and transports in Barrow Strait, the central part of the Northwest Passage, Cont. Shelf Res., 7, 913-935, doi:10.1016/0278-4343(87)90006-9, 1987.

885   Proshutinsky, A., Krishfield, R., Timmermans, M., Toole, J., Carmack, E., McLaughlin, F., Williams, W. J., Zimmermann, S., Itoh, M. and Shimada, K.: Beaufort Gyre freshwater reservoir:

State and variability from observations, J. Geophys. Res. -Oceans, 114, C00A10, doi:10.1029/2008JC005104, 2009.

890   Qi, D., Chen, L., Chen, B., Gao, Z., Zhong, W., Feely, R. A., Anderson, L. G., Sun, H., Chen, J., Chen, M., Zhan, L., Zhang, Y. and Cai, W.: Increase in acidifying water in the western Arctic Ocean, Nat. Clim. Chang., 7, 195-99, doi:10.1038/NCLIMATE3228, 2017.

Robbins, L. L., Wynn, J. G., Lisle, J. T., Yates, K. K., Knorr, P. O., Byrne, R. H., Liu, X., Patsavas, M. C., Azetsu-Scott, K. and Takahashi, T.: Baseline monitoring of the Western Arctic Ocean estimates 20% of Canadian Basin surface waters are undersaturated with respect to aragonite, 895   PLoS One, 8, UNSP e73796, doi:10.1371/journal.pone.0073796, 2013.

Robert-Baldo, G., Morris, M. and Byrne, R.: Spectrophotometric determination of seawater pH using Phenol Red, Anal. Chem., 57, 2564-2567, doi:10.1021/ac00290a030, 1985.

Rodgers, K. B., Lin, J. and Froelicher, T. L.: Emergence of multiple ocean ecosystem drivers in a large ensemble suite with an Earth system model, Biogeosciences, 12, 3301-3320, doi:10.5194/bg-900   12-3301-2015, 2015.

Sabine, C., Feely, R., Gruber, N., Key, R., Lee, K., Bullister, J., Wanninkhof, R., Wong, C., Wallace, D., Tilbrook, B., Millero, F., Peng, T., Kozyr, A., Ono, T. and Rios, A.: The oceanic sink for anthropogenic CO_2, Science, 305, 367-371, doi:10.1126/science.1097403, 2004.

Serreze, M.C. and Barry, R.G.: Processes and impacts of Arctic amplification: A research 905   synthesis, Global Planet. Change, 77, 85-96, doi:10.1016/j.gloplacha.2011.03.004, 2011.

Shadwick, E.H., Thomas, H., Chierici, M., Else, B., Fransson, A., Michel, C., Miller, L. A., Mucci, A., Niemi, A., Papakyriakou, T. N. and Tremblay, J. -E.: Seasonal variability of the inorganic carbon system in the Amundsen Gulf region of the southeastern Beaufort Sea, Limnol. Oceanogr., 56, 303-322, doi:10.4319/lo.2011.56.1.0303, 2011.

910   Shadwick, E.H., Trull, T.W., Thomas, H. and Gibson, J. A. E.: Vulnerability of Polar Oceans to anthropogenic acidification: Comparison of Arctic and Antarctic seasonal cycles, Sci Rep, 3, 2339, doi:10.1038/srep02339, 2013.

Schlitzer, R., Ocean Data View, http://odv.awi.de, 2016.

Stigebrandt, A.: The North Pacific - a Global-Scale Estuary, J. Phys. Oceanogr., 14, 464-470,1984.

915   Stroeve, J. C., Serreze, M. C., Holland, M. M., Kay, J. E., Malanik, J. and Barrett, A. P.: The Arctic's rapidly shrinking sea ice cover: a research synthesis, Clim. Change, 110, 1005-1027, doi:10.1007/s10584-011-0101-1, 2012.

Sutton, A. J., Sabine, C. L., Feely, R. A., Cai, W., Cronin, M. F., McPhaden, M. J., Morell, J. M., Newton, J. A., Noh, J., Olafsdottir, S. R., Salisbury, J. E., Send, U., Vandemark, D. C. and Weller, 920   R. A.: Using present-day observations to detect when anthropogenic change forces surface ocean

carbonate chemistry outside preindustrial bounds, Biogeosciences, 13, 5065-5083, doi:10.5194/bg-13-5065-2016, 2016.

Takahashi, T., Olafsson, J., Goddard, J., Chipman, D. and Sutherland, S.: Seasonal variation of CO_2 and nutrients in the high-latitude surface oceans - a comparative study, Global Biogeochem.
925   Cycles, 7, 843-878, doi:10.1029/93GB02263, 1993.

Tang, C., Ross, C., Yao, T., Petrie, B., DeTracey, B. and Dunlap, E.: The circulation, water masses and sea-ice of Baffin Bay, Prog. Oceanogr., 63, 183-228, doi:10.1016/j.pocean.2004.09.005, 2004.

Tivy, A., Howell, S. E. L., Alt, B., McCourt, S. and Chagnon, R.: Trends and variability in summer sea ice cover in the Canadian Arctic based on the Canadian Ice Service Digital Archive, 1960-
930   2008 and 1968-2008, Journal of Geophysical Research.Oceans, 116, 2011.

Tremblay, J. -E., Belanger, S., Barber, D. G., Asplin, M., Martin, J., Darnis, G., Fortier, L., Gratton, Y., Link, H., Archambault, P., Sallon, A., Michel, C., Williams, W. J., Philippe, B. and Gosselin, M.: Climate forcing multiplies biological productivity in the coastal Arctic Ocean, Geophys. Res. Lett., 38, L18604, doi:10.1029/2011GL048825, 2011.

935   Tremblay, J., Anderson, L. G., Matrai, P., Coupel, P., Belanger, S., Michel, C. and Reigstad, M.: Global and regional drivers of nutrient supply, primary production and CO_2 drawdown in the changing Arctic Ocean, Prog. Oceanogr., 139, 171-196, doi:10.1016/j.pocean.2015.08.009, 2015.

Uppström, L.R.: The boron/chlorinity ratio of deep-sea water from the Pacific Ocean. Deep Sea Research and Oceanographic Abstracts, 21, 161-162, 1974.

940   Wanninkhof, R., Park, G., Takahashi, T., Sweeney, C., Feely, R., Nojiri, Y., Gruber, N., Doney, S. C., McKinley, G. A., Lenton, A., Le Quere, C., Heinze, C., Schwinger, J., Graven, H. and Khatiwala, S.: Global ocean carbon uptake: magnitude, variability and trends, Biogeosciences, 10, 1983-2000, doi:10.5194/bg-10-1983-2013, 2013.

Wolf-Gladrow, D. A., Zeebe, R. E., Klaas, C., Koertzinger, A. and Dickson, A. G.: Total alkalinity:
945   The explicit conservative expression and its application to biogeochemical processes, Mar. Chem., 106, 287-300, doi:10.1016/j.marchem.2007.01.006, 2007.

Wynn, J. G., Robbins, L. L. and Anderson, L. G.: Processes of multibathyal aragonite undersaturation in the Arctic Ocean, J. Geophys. Res. -Oceans, 121, 8248-8267, doi:10.1002/2016JC011696, 2016.

950   Yamamoto-Kawai, M., McLaughlin, F. A. and Carmack, E. C.: Effects of ocean acidification, warming and melting of sea ice on aragonite saturation of the Canada Basin surface water, Geophys. Res. Lett., 38, L03601, doi:10.1029/2010GL045501, 2011.

Yamamoto-Kawai, M., McLaughlin, F. A., Carmack, E. C., Nishino, S., Shimada, K. and Kurita, N.: Surface freshening of the Canada Basin, 2003-2007: River runoff versus sea ice meltwater, J.
955   Geophys. Res. -Oceans, 114, C00A05, doi:10.1029/2008JC005000, 2009a.

Yamamoto-Kawai, M., McLaughlin, F. A., Carmack, E. C., Nishino, S. and Shimada, K.: Aragonite undersaturation in the Arctic Ocean: Effects of ocean acidification and sea ice melt, Science, 326, 1098-1100, doi:10.1126/science.1174190, 2009b.

Zeebe, R. E. and Wolf-Gladrow, D.: Equilibrium, in: CO_2 in Seawater: Equilibrium, kinetics, 960 isotopes. Elsevier Oceanography Series, 65, pp. 346, Amsterdam, 2001.

965

970

Table 1: Research cruises carried out by the CCGS Amundsen from which the

dataset was constructed.

Cruise	Timescale
CASES	September 2003 - August 2004
CFL	September 2007 - July 2008
MALINA	July - August 2009
GEOTRACES	August - September 2009
ARCTICNET Leg 4a	October - November 2009
ARCTICNET	August - September 2013
ARCTICNET	August - September 2014
GEOTRACES / ARCTICNET	July – September 2015
ARCTICNET	August - October 2016

980

Table 2: Mean uncertainties of parameters computed in CO2SYS, their standard deviations and their relative weight with respect to the mean value of each parameter, for different carbonate parameter input pairs. * The ΔDIC_{Bio} uncertainty depends on whether $DIC_{Observed}$ was measured or computed.

985

Computed parameter	Mean uncertainty	Uncertainty standard deviation	% of mean value
pH$_T$ (i-s)	0.026	0.002	0.3
DIC (µmol kg^{-1})	6.8	0.7	0.4
Input Parameters: TA/pH$_T$ (TA/DIC)			
pCO$_2$ (µatm)	6.5 (25.0)	1.8 (6.7)	4.5 (17.5)
Ω$_C$	0.27 (0.13)	0.04 (0.04)	6.5 (3.2)
Ω$_A$	0.16 (0.08)	0.02 (0.02)	6.4 (3.1)
ΔDIC_{Bio} (µmol kg^{-1})	7.8-8.6*	1.3	69-77*

Table 3: Mean surface-water (<10 m) practical salinity (S_P), total alkalinity (TA), dissolved organic

carbon (DIC) and associated ranges in the three sub-regions of the study area in 2014, 2015 and 2016.

	S_P		TA (μmol kg^{-1})		DIC (μmol kg^{-1})	
	mean	range	mean	range	mean	range
Canada Basin	27.52	19.11 - 30.82	2029	1820 - 2231	1929	1761 - 2066
CAA	27.57	22.17 - 31.40	1967	1604 - 2194	1868	1553 - 2061
Baffin Bay	30.96	29.69 - 32.10	2138	2062 - 2209	1999	1920 - 2058

990

995
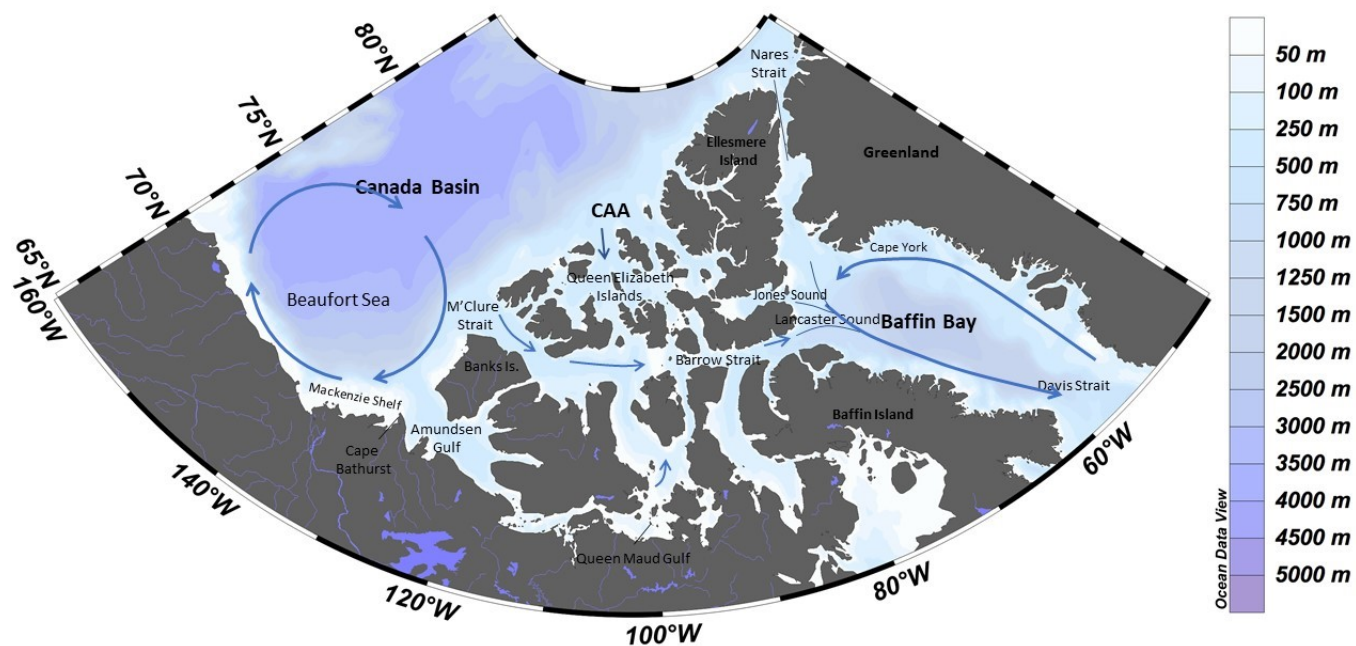
Figure 1: Map of the study area with dominant surface circulation flow paths. After McLaughlin et al. (2004) and Proshutinsky et al. (2009). CAA: Canadian Arctic Archipelago. Created using Ocean Data View (Schlizter, 2016)

1000

1005
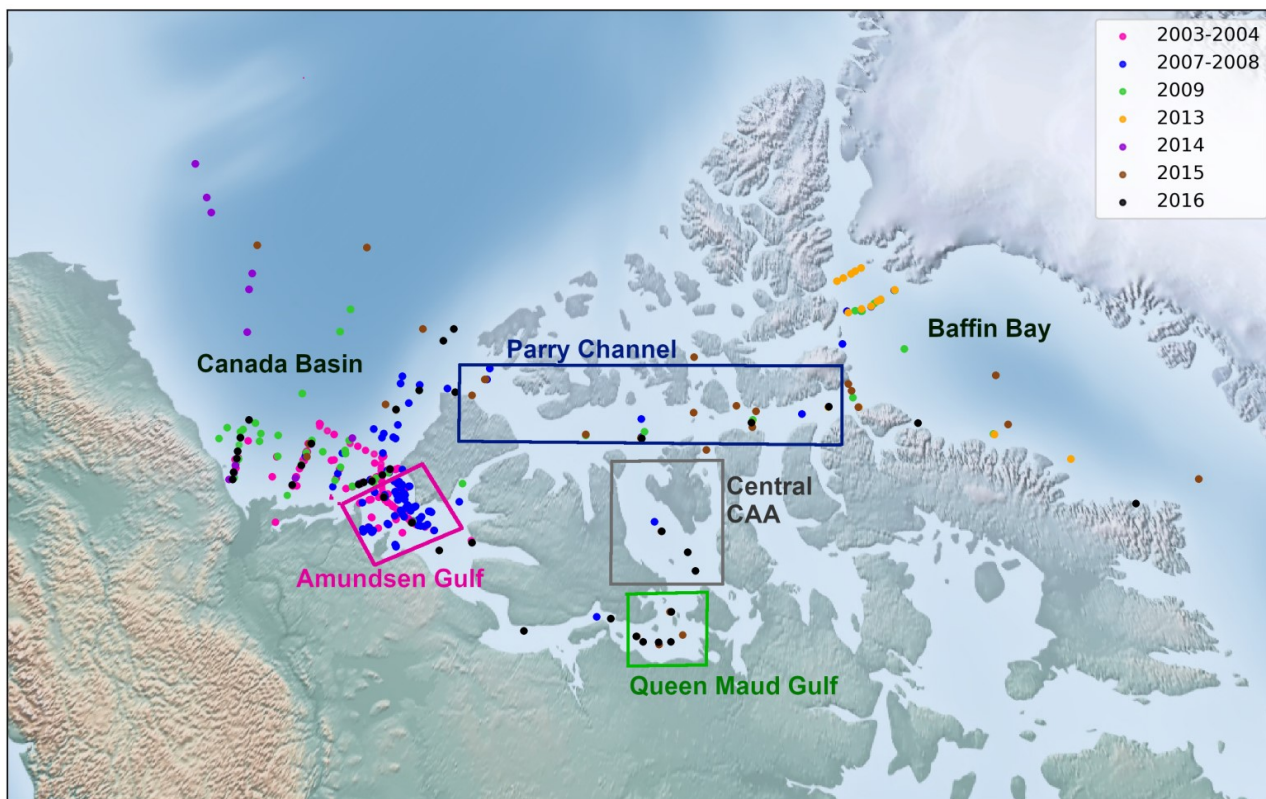
Figure 2: Geographical location of the oceanographic stations covered by the dataset, color-coded according to the year of sampling, with the approximate boundaries of the main areas mentioned in the text.

1010
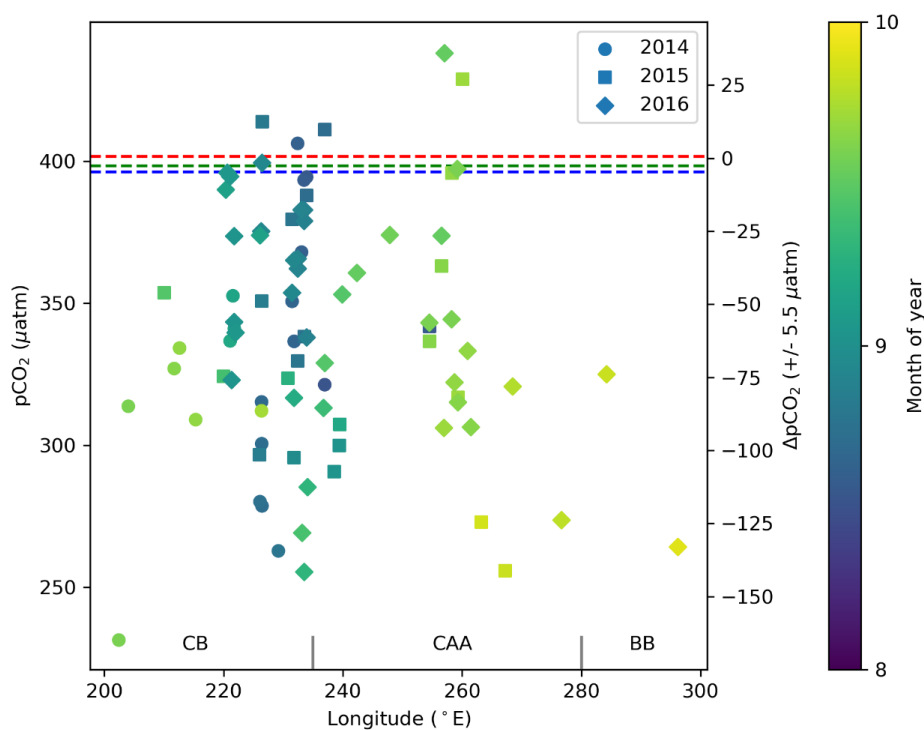
Figure 3: Surface-water (<5m) pCO_2 and ΔpCO_2 ($pCO_{2SW} - pCO_{2air}$) from 2014, 2015 and 2016 in the Canada Basin (CB), Canadian Arctic Archipelago (CAA) and Baffin Bay (BB). The blue, green and red dashed lines represent the average of the global mean monthly atmospheric pCO_2 values for August and September 2014, 2015 and 2016, respectively (data from Dlugokencky and Tans, NOAA/ESRL). The ΔpCO_2 axis shifts in accordance with the atmospheric value used for each year, such that points may be offset from their true position by up to 5.5 µatm.
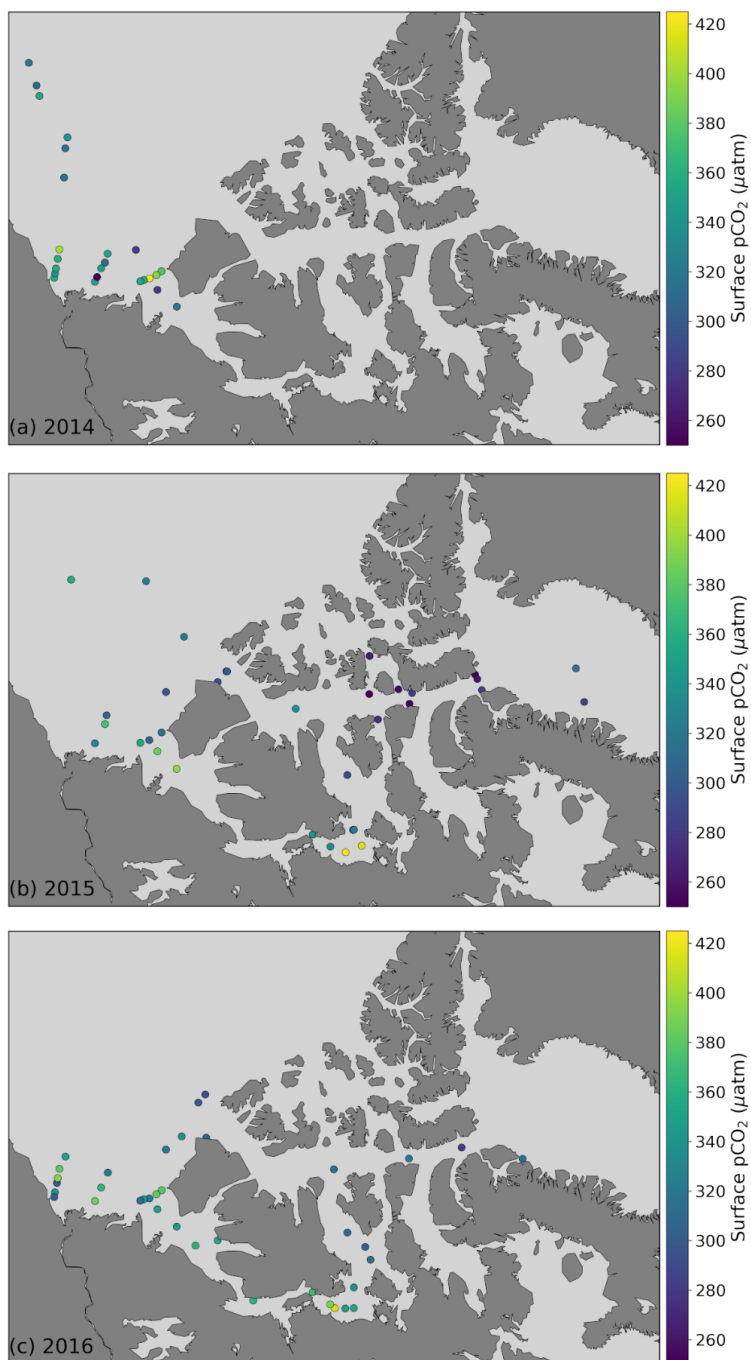
Figure 4: Surface-water (<5m) pCO_2 in 2014 (a), 2015 (b) and 2016 (c).
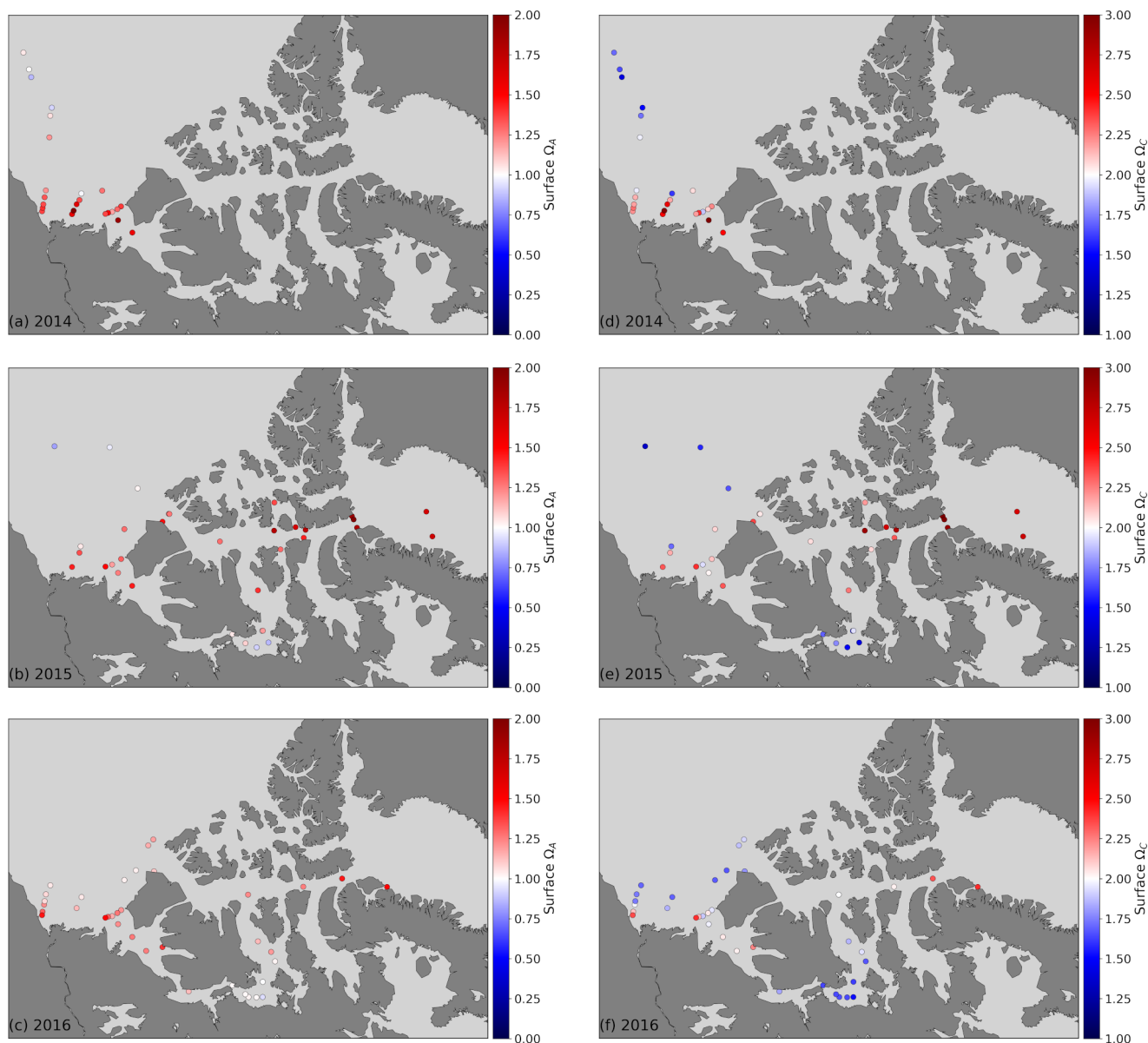
Figure 5: Surface-water (< 10m) Ω_A (left) and Ω_C (right) in 2014 (top), 2015 (middle) and 2016 (bottom). Note the different color scales for Ω_A and Ω_C, for which the diverging value for the former is 1, 2 for the latter.

1030
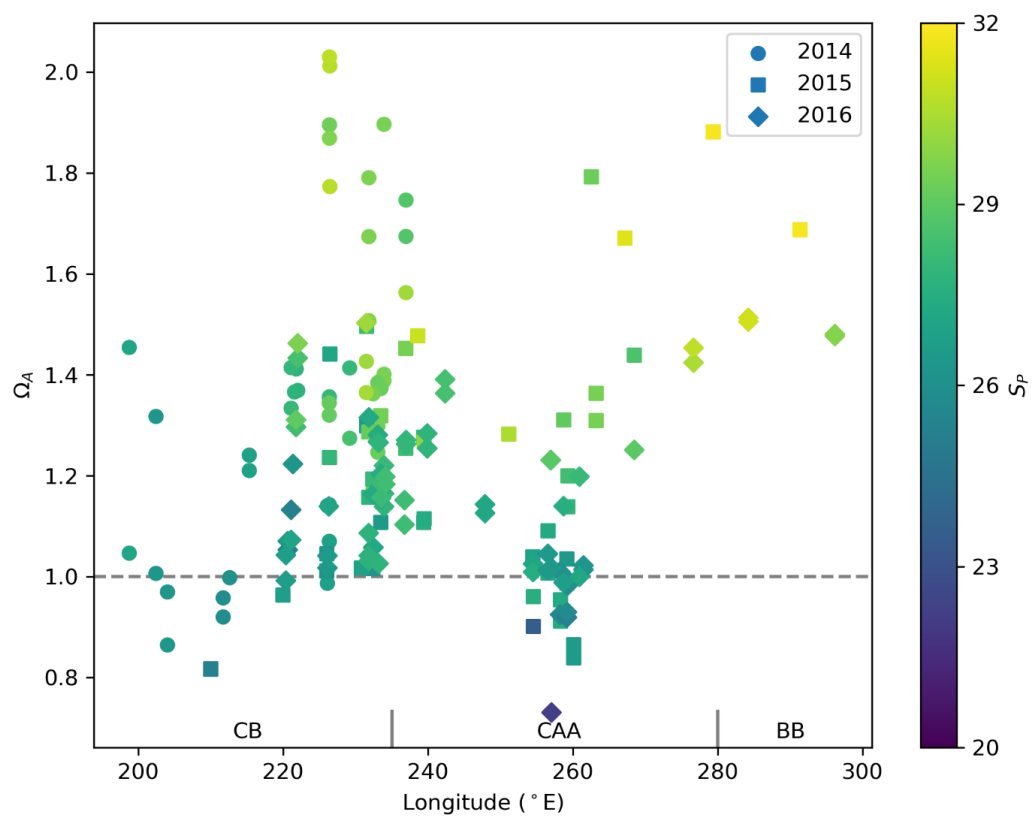
Figure 6: Surface-water (< 10m) Ω_A and associated practical salinities (S_P, color scale) in 2014,
2015 and 2016 in the Canada Basin (CB), Canadian Arctic Archipelago (CAA) and Baffin Bay
(BB). The horizontal line at $\Omega_A = 1$ represents saturation with respect to aragonite.

1035
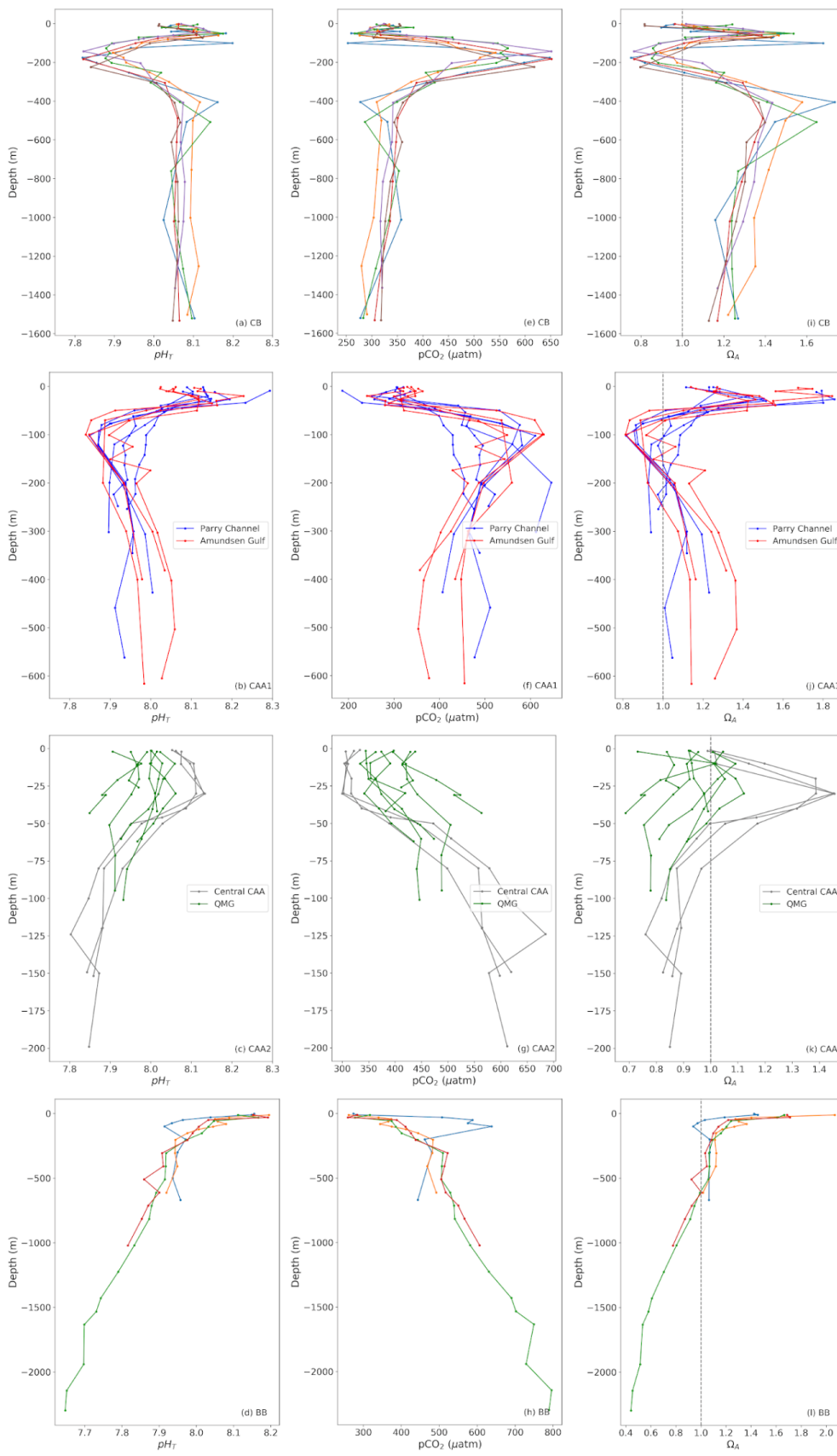
Figure 7: Depth profiles of pH_T (left), pCO_2 (middle) and Ω_A (right) at representative stations of the Canada Basin (CB; top), Baffin Bay (BB; bottom) and the Canadian Arctic Archipelago (CAA). The latter is divided into 4 sub-regions (shown on Fig. 2): Parry Channel, Amundsen Gulf, Central Archipelago and Queen Maud Gulf (QMG).

1040
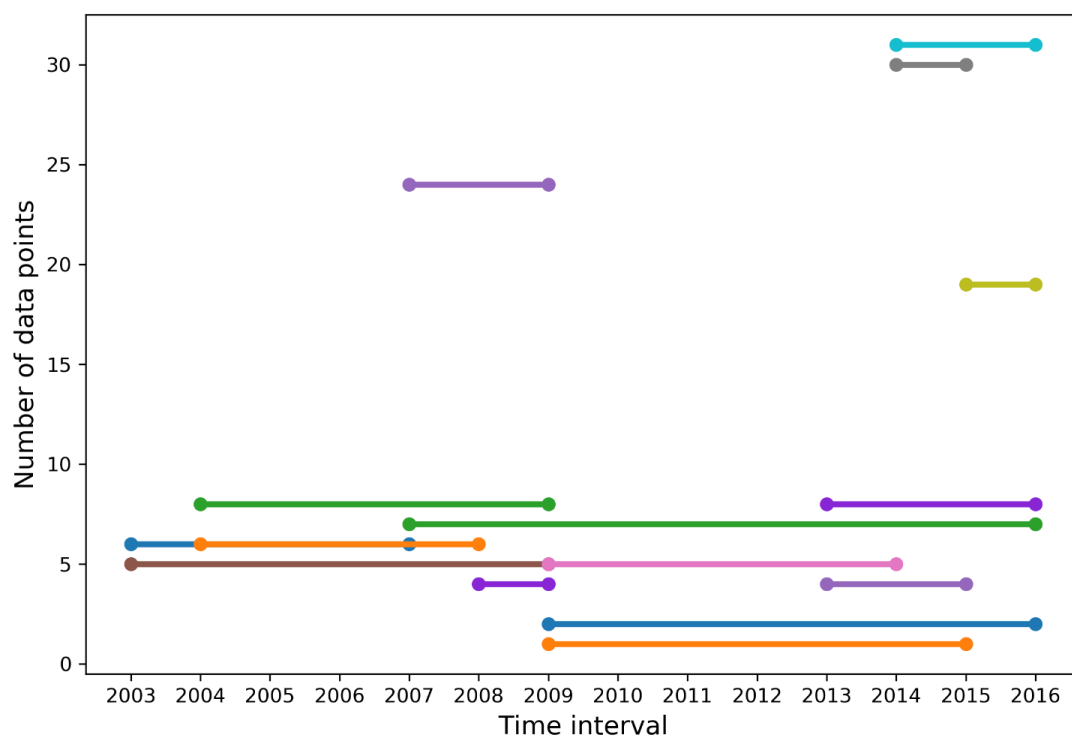
Figure 8: Number of comparable data points in the top 100m of the water column, obtained from measurements made at the same station and within set depth intervals (of 3.5 meters at the surface, increasing progressively to 15 m to a depth of 100 m), between each year of the dataset.

1045
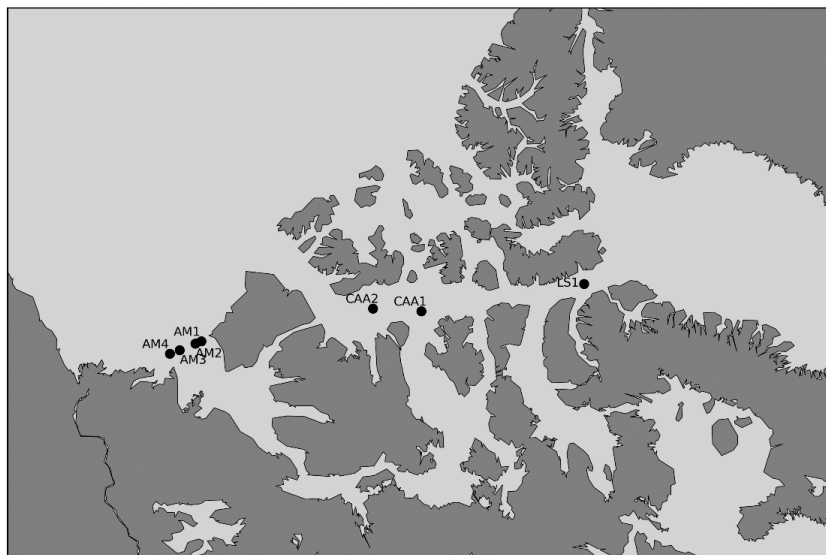
Figure 9: Location of the stations visited over an interval of 5 years or more. Stations are designated by area-related acronyms (LS: Lancaster Sound, CAA: Canadian Arctic Archipelago, AM: Amundsen Gulf), that are not the station identifiers used during the expeditions.
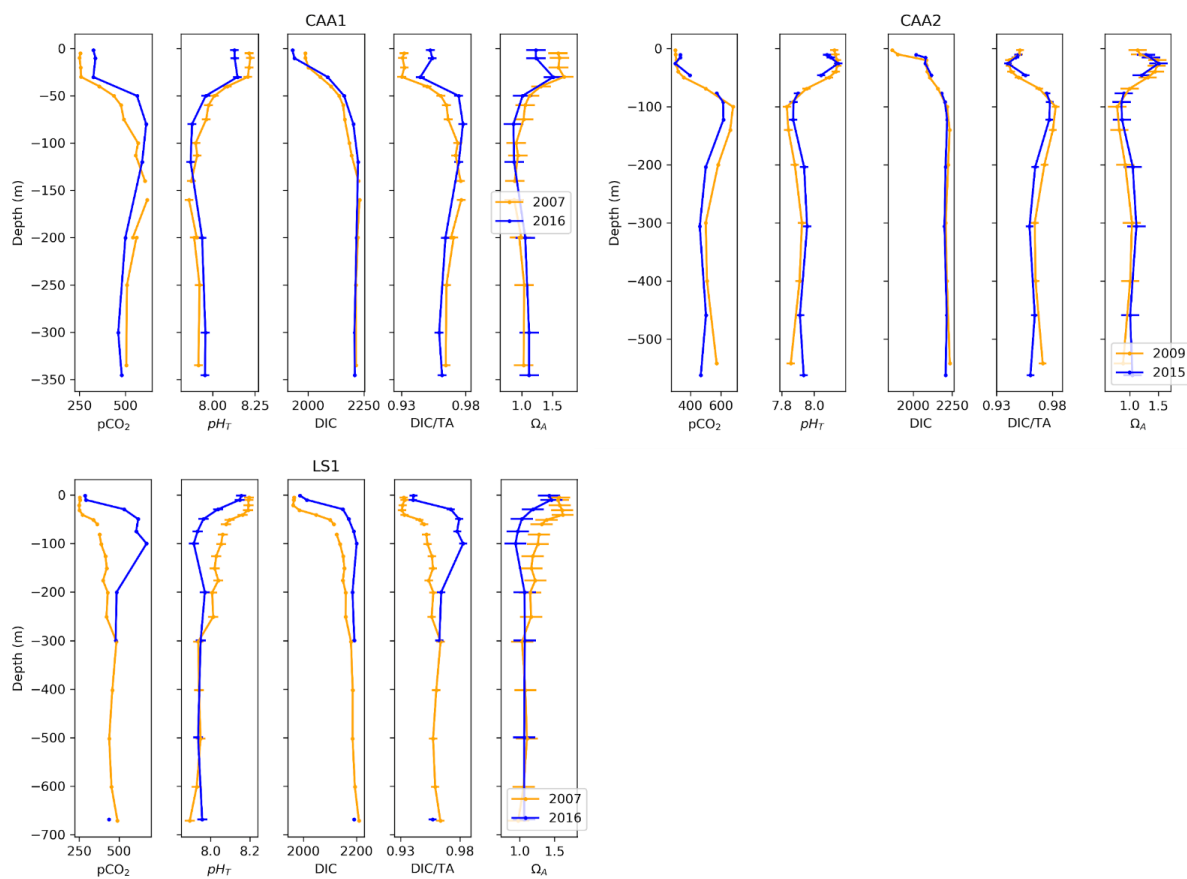
Figure 10: Depth profiles of pCO$_2$, pH$_T$, DIC, DIC/TA and Ω_A across time at one location in Lancaster Sound (LS1) and two locations in the Canadian Arctic Archipelago (CAA1, CAA2).

1055
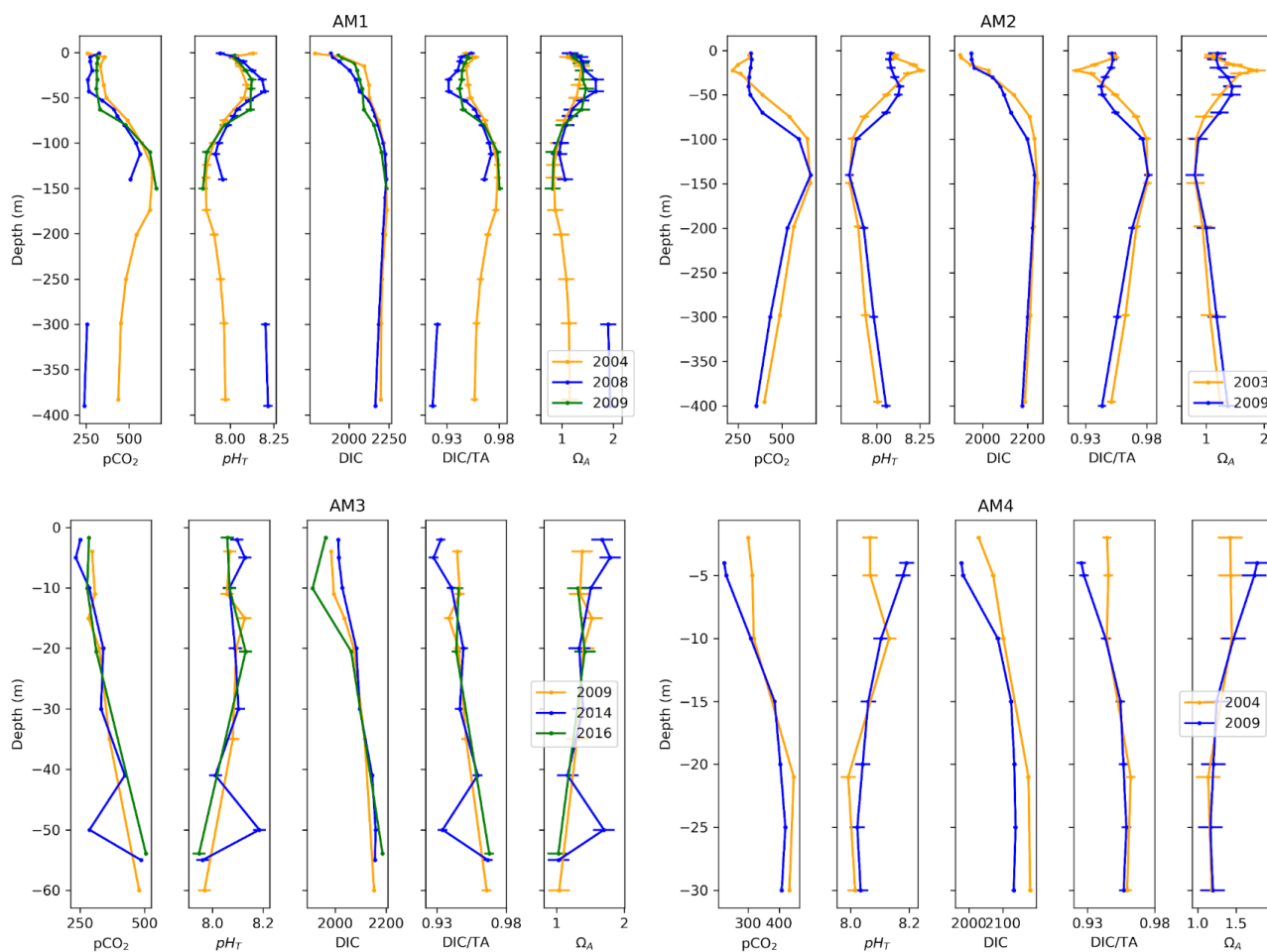
Figure 11: Depth profiles of pCO_2, pH_T, DIC, DIC/TA and Ω_A and uncertainties across time at four locations at the western limit of the Amundsen Gulf (AM1,2,3,4).

1060

1065

1070

1075
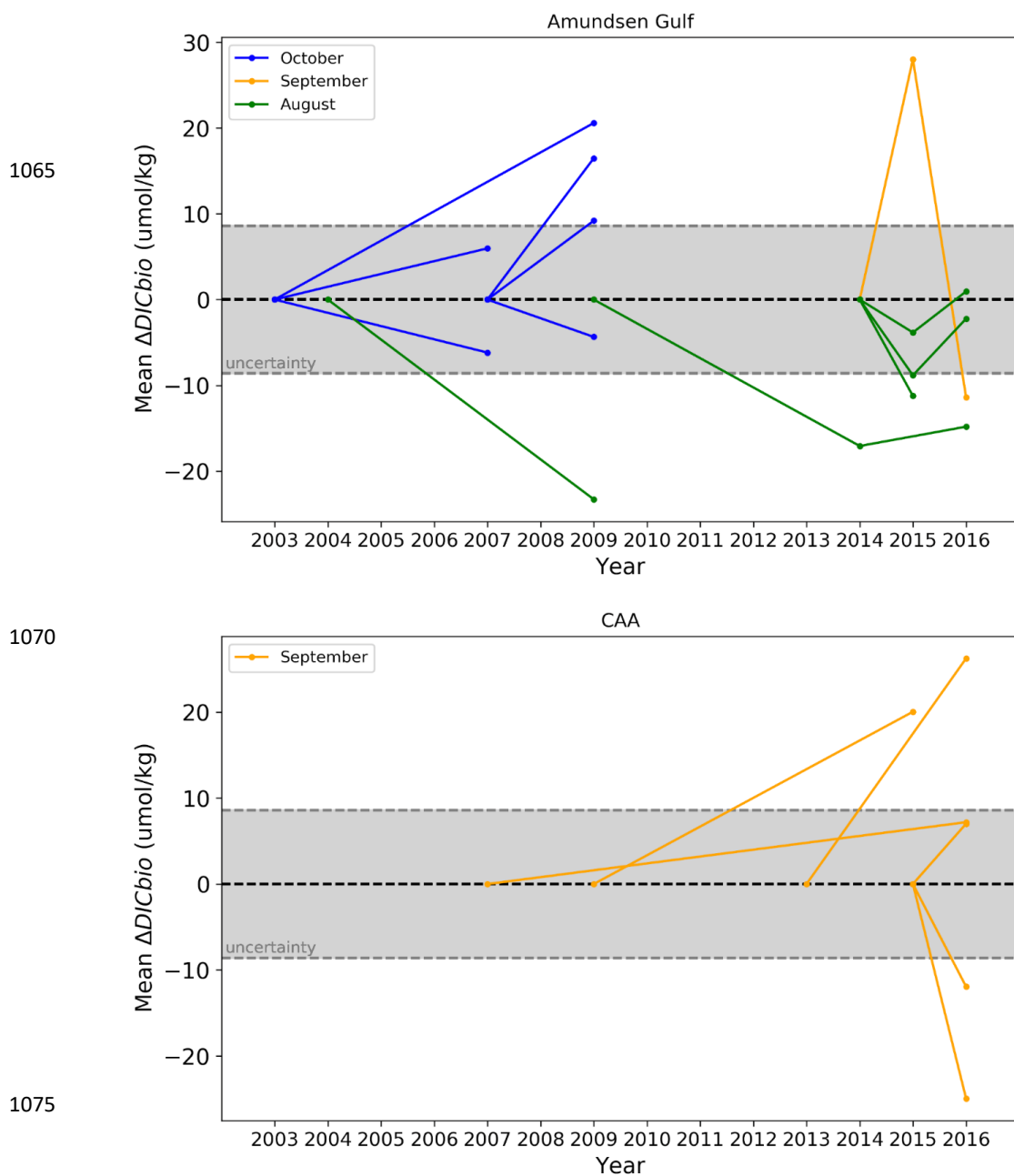
Figure 12: Mean ΔDIC_{Bio} (top 25 meters of the water column) at stations of the Amundsen Gulf (top) and Canadian Arctic Archipelago (bottom). The central dashed line (0) is the reference state, in relation to which ΔDIC_{Bio} is expressed (i.e. the point at the right extremity of a line indicates the ΔDIC_{Bio} relative to the year at which this line intersects the zero dashed line). The grey shaded area represents the range of uncertainty.

Table A1: Values of natural variability (N; the standard deviation of the annual means of each

1080   parameter) and theoretical acidification rate (S; the slope of the theoretical acidification curve)

used in the time of emergence calculations.

Parameter	N	S
pH (i-s)	0.025	-0.002 yr^{-1}
pCO$_2$	26.65 µatm	2.17 µatm yr^{-1}
Ω_A	0.07	-0.004 yr^{-1}
DIC	36.37 µmol kg^{-1}	0.61 µmol kg^{-1} yr^{-1}

1085

1090

1095

Biogeosciences
Discussions
Open Access
EGU

Table A2: Calculated times of emergence of carbonate system parameters at various depths, rounded to the closest year. The C value represents the threshold used (2 or 3 standard deviations of annual means).

1100

Parameter		Time of Emergence (Years)		
		0 – 15 m	90 – 110 m	290 – 310 m
pH (i-s)	C = 2	23	26	21
	C = 3	35	40	31
pCO$_2$	C = 2	25	36	20
	C = 3	37	55	29
Ω$_A$	C = 2	31	31	20
	C = 3	46	46	29
DIC	C = 2	118	156	138
	C = 3	177	234	207

1110

1115

Table A3: Number of data points included in the annual means used in the time of emergence calculations.

Year	Data Count		
	0 – 15 m	90 - 110 m	290 – 310 m
2003	166	30	15
2004	207	47	22
2007	65	24	10
2008	146	66	31
2009	103	17	10
2014	63	20	16
2015	24	10	5

1120